

THESIS

TUNING SURFACE WETTABILITY FOR EFFECTIVE OIL-WATER SEPARATION,  
MANIPULATION OF FERROFLUID DROPLETS AND BLOOD CONTACTING MEDICAL  
DEVICES

Submitted by

Prem Kantam

Department of Mechanical Engineering

In partial fulfillment of the requirements

For the Degree of Master of Science

Colorado State University

Fort Collins, Colorado

Spring 2020

Master's Committee:

Advisor: Arun K. Kota

Co-Advisor: Ketul C. Popat

Vivian Li

Copyright by Prem Kantam 2020

All Rights Reserved

## ABSTRACT

### TUNING SURFACE WETTABILITY FOR EFFECTIVE OIL-WATER SEPARATION, MANIPULATION OF FERROFLUID DROPLETS AND BLOOD CONTACTING MEDICAL DEVICES

Surface interaction with liquids have gained a lot of attention that enables us to control wetting properties which find applications in self-cleaning, stain free clothing, non-fouling, separation of liquids etc. In this study we tuned surface wettability of different surfaces to showcase potential applications in oil-water separation, manipulation of under liquid droplets and blood contacting medical devices.

First, we designed dual superlyophobic surfaces by combining re-entrant texture and appropriate surface energy with recently discovered recyclable polymer. Dual superlyophobic surfaces display both under-water superoleophobicity and underoil superhydrophobicity. Such surfaces are counter-intuitive because typically underwater superoleophobic surfaces require high surface energy and under-oil superhydrophobic surfaces require low surface energy. We fabricated these surfaces using a simple spray coating method that resulted in textured surface with re-entrant structures. The surface energy of the textured surfaces was then modified through plasma treatment. Our surfaces display under-water superoleophobicity for low surface tension liquids liker oils and under-oil superhydrophobicity for high surface tension liquids like water. We envision that our dual superlyophobic surfaces will find applications in membrane separation, antifouling coatings and droplet-based fluidic devices.

Second, we developed polyethylene glycol based hydrophilic slippery surfaces by covalently attaching PEG silane via O-Si bonds to hydroxylated surface to form PEG brushes. The hydrophilic slippery surfaces formed are chemically homogeneous with low molecular weight PEG

brushes with high grafting density. These surfaces can easily repel high surface tension liquids like water and blood with a tilt angle of  $6^\circ$ . It is envisioned that these surfaces can be effectively used to reduce protein adsorption, platelet adhesion and bacterial adhesion and the use of slippery surfaces can be an ideal approach for designing surfaces for blood-contacting medical devices.

## ACKNOWLEDGEMENTS

I want to thank my advisor Dr. Arun Kota for his continuous support, assistance and guidance towards my thesis. I want to thank Dr. Ketul C. Popat and Dr. Vivian Li for being a part of my thesis committee and their support in completion of my thesis and master's degree. I want to thank Dr Wei Wang for his continuous support throughout this project. I want to thank Sravanthi Vallabhuneni and Vignesh Manivasagam for their help with SEM and their timely suggestions towards my projects. I want to thank Dr. Hamed Vahabi, Dan Sutherland, Shou Liu, and Harvinder Singh Virk for their valuable inputs and constant discussions during regular group meetings. I want to thank Roberta Sabino and Sayudh Ghosh for their continuous support and valuable inputs towards my thesis. I want to acknowledge NSF and NIH for their financial support in funding the projects.

## TABLE OF CONTENTS

ABSTRACT.....	ii
ACKNOWLEDGEMENTS .....	iv
LIST OF TABLES.....	vii
LIST OF FIGURES .....	viii
<b>INTRODUCTION .....</b>	<b>1</b>
<b>HYPOTHESIS AND SPECIFIC AIMS .....</b>	<b>3</b>
<b>CHAPTER 1 .....</b>	<b>4</b>
<b>INTRODUCTION TO WETTABILITY.....</b>	<b>4</b>
1.1 Contact Angle (CA) .....	4
1.2 Contact Angle Hysteresis (CAH).....	5
1.3 Sliding Angles or Roll off Angles .....	6
1.4 Textured Surfaces: Cassie and Wenzel state of wetting.....	6
1.5 Super Repellent Surfaces and the need for Re-entrant texture .....	8
<b>CHAPTER 2 .....</b>	<b>10</b>
<b>Dual Superlyophobic Surfaces with Recyclable Polymer .....</b>	<b>10</b>
2.1 Introduction.....	10
2.2 Materials.....	12
2.3 Methods .....	12
2.3.1 <i>Fabrication of Dual Superlyophobic Surfaces</i> .....	12
2.3.2 <i>Surface characterization of Dual Superlyophobic surfaces</i> .....	13
2.3.3 <i>Surface Wettability of Dual Superlyophobic surfaces</i> .....	13
2.3.4 <i>Surface Energy of the recyclable polymer</i> .....	13
2.4 Results and Discussions .....	14
2.5 Applications .....	18
2.5.1 <i>Manipulation of underwater ferrofluid droplets</i> .....	18
2.5.2 <i>Oil/water Separation</i> .....	20
<b>PEGylated hydrophilic slippery surfaces for low protein adsorption, platelet adhesion and activation and bacterial adhesion.....</b>	<b>22</b>
3.1 Introduction.....	22
3.2 Methods .....	24
3.2.1 <i>Fabrication of PEGylated hydrophilic slippery surfaces</i> .....	24
3.2.2 <i>Surface characterization of PEGylated hydrophilic slippery surfaces</i> .....	25

3.2.3 Protein adsorption on PEGylated hydrophilic slippery surfaces .....	26
3.2.4 Isolation of Platelet rich plasma (PRP) from whole human blood.....	27
3.2.5 Cytotoxicity on PEGylated hydrophilic surfaces .....	27
3.2.6 Cell adhesion on PEGylated hydrophilic slippery surfaces .....	27
3.2.7 Identification of platelets and leukocytes adhered on PEGylated hydrophilic slippery surfaces .....	28
3.2.8 Platelet activation on PEGylated hydrophilic slippery surfaces .....	28
3.2.9 Whole human blood clotting on PEGylated hydrophilic slippery surfaces .....	29
3.2.10 Preparation of bacteria culture.....	29
3.2.11 Anti-bacterial activity on PEGylated hydrophilic slippery surfaces.....	30
3.2.12 Statistical Analysis .....	31
3.3 Results and Discussion .....	31
<b>CHAPTER 4 .....</b>	<b>46</b>
<b>Conclusions and Future Work .....</b>	<b>46</b>
4.1 Conclusions .....	46
4.2 Future Work.....	46
<b>References .....</b>	<b>48</b>

## LIST OF TABLES

Table 1: Elemental composition of PEGylated and unmodified surfaces .....	33
Table 2: Elemental composition of carbon groups on PEGylated and unmodified surfaces.....	33
Table 3: Table representing the wettability properties on PEGylated and unmodified surfaces ...	34

## LIST OF FIGURES

Figure 1. Schematic indicating the equilibrium contact angle ( $\theta_v$ ) of a liquid drop in contact with a non-textured, non-reactive ideally smooth surface through a force balance (Image reproduced from Dr. Kota's lectures). .....	4
Figure 2. Schematic illustrating the advancing (maximum) and receding (minimum) contact angles of a liquid drop on a smooth surface (Image reproduced from Dr. Kota's lectures).....	5
Figure 3. Schematic illustrating the sliding angle ( $\alpha$ ) of a liquid droplet on a smooth surface (Image reproduced from Dr. Kota's lectures).....	6
Figure 4. Schematic illustrating apparent contact angle of liquid droplet ( $\theta^*$ ) in Wenzel state (Image reproduced from Dr. Kota's lectures).....	7
Figure 5. Schematic illustrating apparent contact angle of liquid droplet ( $\theta^*$ ) in Cassie-Baxter state (Image reproduced from Dr. Kota's lectures). .....	8
Figure 6. Schematic illustrating a) liquid droplet on a textured surface with texture angle $>90^\circ$ for $\Theta > 90^\circ$ in Cassie state. b) liquid drop on a textured surface with texture angle $<90^\circ$ (re-entrant texture) for $\Theta < 90^\circ$ in Cassie state (Image reproduced from Dr. Kota's lectures). .....	9
Figure 7. Schematic illustrating the fabrication of Dual Superlyophobic surfaces .....	13
Figure 8. a) SEM images of the dual superlyophobic surfaces b) Static contact angle of a water droplet (hydrophilic) in air on dual superlyophobic surface c) Static contact angle of a hexadecane droplet (superoleophilic) in air on dual superlyophobic surface. ....	14
Figure 9. a) Underwater oleophobicity of various low surface tension liquids on smooth surfaces b) Underwater superoleophobicity of various low surface tension liquids on textured surfaces c) Roll off angle of a krytox droplet underwater. ....	15
Figure 10. Underwater apparent contact angles and roll off angles of all low surface tension liquids. ....	16

Figure 11. a) Under-oil hydrophobicity of various water-ethanol mixtures on smooth surfaces b) Under-oil superhydrophobicity of various water-ethanol mixtures on textured surfaces c) Roll off angle of a water droplet under-oil.....17

Figure 12. Underoil apparent contact angles and roll off angles for water and water-ethanol mixtures. ....17

Figure 13. a) Oil based ferro fluid on the dual superlyophobic surface underwater. b, c, d) Figure indicating the motion and splitting of ferro fluid on the dual superlyophobic surface with external magnetic field.....19

Figure 14. a-c) Separation of water from hexadecane-water mixture using dual superlyophobic membrane. e-f) Separation of krytox from krytox-water mixture using dual superlyophobic membrane.....21

Figure 15. Schematic illustrating the fabrication of PEGylated hydrophilic slippery surfaces where R represents methyl groups .....25

Figure 16. a) Survey scans for PEGylated and unmodified surfaces. b) High resolution scan for the PEGylated surface. c) High resolution scan for the unmodified surface.....33

Figure 17. a) Albumin adsorption on unmodified and PEGylated surfaces. b) Fibrinogen adsorption on unmodified and PEGylated surfaces. ....36

Figure 18. Absorbance values representing cell cytotoxicity of surfaces exposed to PRP .....36

Figure 19. a) Fluorescence microscopy images indicating cell (Live) adhesion from PRP on unmodified and PEGylated surfaces. b) Percentage area of cells adhered on unmodified and PEGylated surfaces using ImageJ. ....38

Figure 20. a) Fluorescence microscopy images indicating platelets and leukocytes adhesion using DAPI and Rhodamine-Phalloidin stain on unmodified and PEGylated surfaces. b) Percentage area of adhered platelets and leukocytes on unmodified and PEGylated surfaces using ImageJ. ....39

Figure 21. Scanning electron microscope images of leukocytes and platelets adhesion on unmodified and PEGylated surfaces. ....40

Figure 22. Whole human blood clotting on unmodified and PEGylated surfaces after 15, 30 and 45mins (dashed line indicates the amount of free haemoglobin in un-clotted blood). ....41

Figure 23a) Fluorescence microscopy images indicating bacterial adhesion (E. Coli) on the surfaces after 6 hrs and 24 hrs of incubation. b) Percentage area of Live and Dead E Coli adhered on the surfaces. ....43

Figure 24. a) Fluorescence microscopy images indicating bacterial adhesion (S Aureus) on the surfaces after 6 hrs and 24 hrs of incubation. b) Percentage area of Live and Dead S. Aureus adhered on the surfaces. ....44

Figure 25. Scanning electron microscopy images indicating bacterial adhesion (E. Coli) on the surfaces after 6 hrs and 24 hrs of incubation.....45

Figure 26. Scanning electron microscopy images indicating bacterial adhesion (S. Aureus) on the surfaces after 6 hrs and 24 hrs of incubation.....45

## INTRODUCTION

Surface interaction with liquids have gained a lot of attention that enables us to control wetting properties which find applications in self-cleaning, stain free clothing, non-fouling, separation of liquids etc. This research work emphasizes on tuning surface wettability of different surfaces to show potential applications in effective oil-water separation, manipulation of ferrofluid droplets and blood contacting medical devices.

Dual superlyophobic surfaces display both under-water superoleophobicity and underoil superhydrophobicity. Such surfaces are counter-intuitive because typically underwater superoleophobic surfaces require high surface energy and under-oil superhydrophobic surfaces require low surface energy. We fabricated dual superlyophobic surfaces using a recyclable polymer in this study. We showcased potential application in oil-water separation and manipulation of ferrofluid droplets. The field of oil-water separation plays a significant role in resolving potential industrial concerns over oil-water pollution<sup>1-3</sup>. It is in fact a challenge to remove toxic contaminants with high efficiency and low energy consumption. As of today, there have been many novel materials that have been reported to tackle such problems. However, fabrication of these membranes for effective oil-water separation have been reported using complex fabrication techniques, expensive reagents and instruments. We report fabrication of these dual superlyophobic surfaces from recyclable polymer using a simple spray coating technique which can be used as a membrane for effective oil-water separation which is discussed in chapter 2. Further manipulation of aqueous droplets finds various applications in microfluidics, cell sorting and biochemical analysis. Droplet based microfluidics result in droplet mixing, separation, transport etc., which enhances control over individual droplets. This research also emphasizes the use of dual superlyophobic surfaces to showcase potential manipulation of ferrofluids underwater which is further discussed in chapter 2.

Next in this research, we fabricated PEGylated hydrophilic slippery surfaces to showcase the use of slipperiness as an ideal approach to design surfaces for blood contacting medical devices. When a biocompatible material encounters blood, fibrinogen gets adsorbed onto the surface which forms the basis for coagulation cascade<sup>4,5</sup>. The adsorbed fibrinogen further instigate platelet, leukocyte and bacterial adhesion which leads to problems related to blood clotting thrombosis leading to the failure of the device<sup>4</sup>. Hence it is important to study blood-material interactions to understand the underlying mechanisms which lead to better design of blood contacting materials. It is envisioned that the PEGylated slippery surfaces can be effectively used to reduce protein adsorption, platelet adhesion and bacterial adhesion and the use of slippery surfaces can be an ideal approach for designing surfaces for blood-contacting medical devices. The biological studies and the results are further discussed in chapter 3.

## HYPOTHESIS AND SPECIFIC AIMS

**Hypothesis 1:** Dual superlyophobic surfaces can be fabricated by appropriate re-entrant texture and careful modification of surface energy. These surfaces find applications in effective oil-water separation and manipulation of under-liquid ferrofluid droplets.

**Specific aim 1:** Fabrication, characterization and applications on dual superlyophobic surfaces discussed in chapter 2 will tell:

- i) Fabrication of the dual superlyophobic surfaces from recyclable polymer.
- ii) Characterization of dual superlyophobic surfaces in terms of SEM and wettability.
- iii) Demonstrating potential applications on dual superlyophobic surfaces.

**Hypothesis 2:** PEGylated hydrophilic surfaces can reduce protein adsorption, platelet adhesion and activation and bacterial adhesion.

**Specific aim 2:** Fabrication, characterization and biological studies on PEGylated hydrophilic slippery surfaces discussed in chapter 3 will tell:

- i) Fabrication of PEGylated hydrophilic slippery surfaces.
- ii) Characterization of PEGylated hydrophilic surfaces in terms of SEM and XPS.
- iii) Results obtained from all the biological studies and comparison of these surfaces with the unmodified surfaces.

## CHAPTER 1

### INTRODUCTION TO WETTABILITY

Surface Wettability is an important factor that quantifies how a liquid behaves when it interacts with a solid surface. Over the years surface wettability has enhanced researches to develop surfaces that find many commercial and military applications like drag reduction, heat transfer, anti-fouling, microfluidics, self-cleaning, blood contacting medical devices etc<sup>6-11</sup>. Wettability for a given surface is typically characterised by Contact Angle (CA) and Contact Angle Hysteresis(CAH)<sup>6,12,13</sup>.

#### 1.1 Contact Angle (CA)

On a non-reactive, non-textured and ideally smooth surface, equilibrium contact angle is defined as the angle between the tangent to solid-liquid interface and the tangent to liquid-vapor interface at the triple phase contact line measuring through the liquid<sup>6</sup>. The equilibrium contact angle ( $\theta$ ) is given by the Young's relation as<sup>14</sup>:

$$\cos(\theta) = (\gamma_{sv} - \gamma_{sl})/\gamma_{lv} \quad (1)$$

where  $\gamma_{sl}$  is the solid liquid interfacial tension,  $\gamma_{sv}$  is the solid surface energy and  $\gamma_{lv}$  is the liquid surface tension.

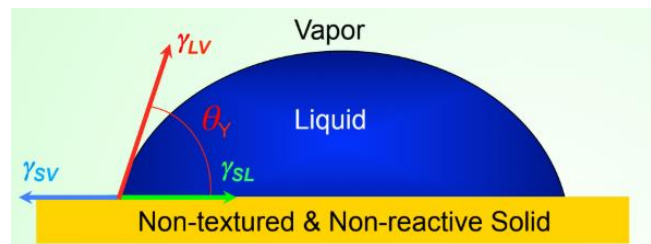


*Figure 1. Schematic indicating the equilibrium contact angle ( $\theta_Y$ ) of a liquid drop in contact with a non-textured, non-reactive ideally smooth surface through a force balance (Image reproduced from Dr. Kota's lectures).*

Taking water droplet into consideration, surfaces are termed superhydrophilic ( $\theta \sim 0^\circ$ ), hydrophilic ( $0^\circ < \theta < 90^\circ$ ) and hydrophobic ( $\theta > 90^\circ$ ). Similarly taking low surface tension liquid like an oil, surfaces can be classified into superoleophilic when  $\theta \sim 0^\circ$ , oleophilic when  $0^\circ < \theta < 90^\circ$  and oleophobic when  $\theta > 90^\circ$ .

From the Young's relation it is clear that, surfaces with higher surface energy display lower contact angles and surfaces with lower surface energy display higher contact angles<sup>6</sup>. Hence low surface energy materials are desired for displaying higher contact angles.

### 1.2 Contact Angle Hysteresis (CAH)

Another important factor that quantifies wettability is contact angle hysteresis<sup>9</sup>. Contact angle hysteresis is the measure of energy dissipated when a liquid moves along a solid surface<sup>15</sup>. Mathematically it is defined as the difference between the advancing (maximum) contact angle and the receding (minimum) contact angle of a liquid on a given surface<sup>6</sup>. It is given by:

$$\Delta \theta = \theta_{adv} - \theta_{rec} \quad (2)$$

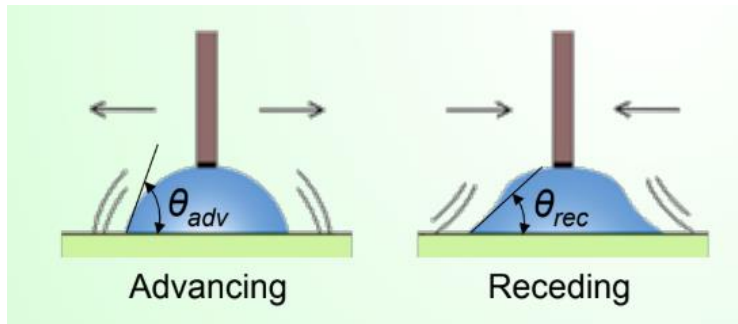


Figure 2. Schematic illustrating the advancing (maximum) and receding (minimum) contact angles of a liquid drop on a smooth surface (Image reproduced from Dr. Kota's lectures).

Contact angle hysteresis arises due to texture and chemical inhomogeneities on the surface. For a given surface, lower contact angle hysteresis indicates higher mobility of the droplet which results in lower solid liquid interfacial area between the liquid droplet and solid surface. On the

other hand, higher contact angles hysteresis due to texture and chemical inhomogeneities lead to lower mobility of the droplet which results in higher solid liquid interfacial area between the liquid droplet and the solid surface.

### 1.3 Sliding Angles or Roll off Angles

The sliding or roll off angle is defined as the minimum angle by which the surface must be tilted in relation to the horizontal so as the liquid drop slides or rolls off the solid surface. It is denoted by  $\alpha$  and is given by Furmidge<sup>16</sup> relation as:

$$\sin \alpha = \gamma_{lv} w (\cos \theta_{rec} - \cos \theta_{adv}) / \rho g V \quad (3)$$

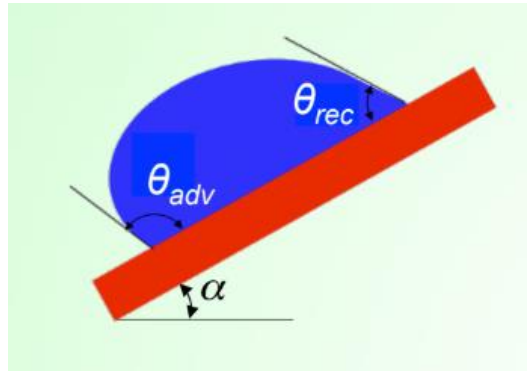


Figure 3. Schematic illustrating the sliding angle ( $\alpha$ ) of a liquid droplet on a smooth surface (Image reproduced from Dr. Kota's lectures).

where  $\gamma_{lv}$  is the surface tension of the liquid,  $\alpha$  is the sliding or roll off angle,  $w$  is width of the liquid droplet,  $V$  is the volume of the liquid droplet used,  $g$  is the acceleration due to gravity and  $\rho$  is the density of the liquid used.

### 1.4 Textured Surfaces: Cassie and Wenzel state of wetting

The wettability of a liquid droplet on a textured surface differs from a smooth surface. The measured or macroscopic contact angle on a textured surface is defined as the apparent contact angle which is denoted by  $\theta^*$ . When the liquid droplet comes into contact with a textured surface,

it adapts either the Wenzel state or Cassie Baxter State to minimize its overall free energy<sup>6,17,18</sup>. In Wenzel state, the liquid droplet completely penetrates into the texture of the surface thereby having a completely wetted interface and the apparent contact angles are determined by using the relation<sup>17</sup>:

$$\cos\theta^* = r\cos\theta \quad (4)$$

where  $r$  is the surface roughness of the surface which is the ratio of actual solid liquid interfacial area to the projected surface area. Due to roughness, Wenzel state enhances wetting or de-wetting. If  $\theta < 90^\circ$  then  $\theta^* \ll 90^\circ$  and if  $\theta > 90^\circ$  then  $\theta^* \gg 90^\circ$ . Roughness can be of any shape such as cylinders, pillars, ridges etc.

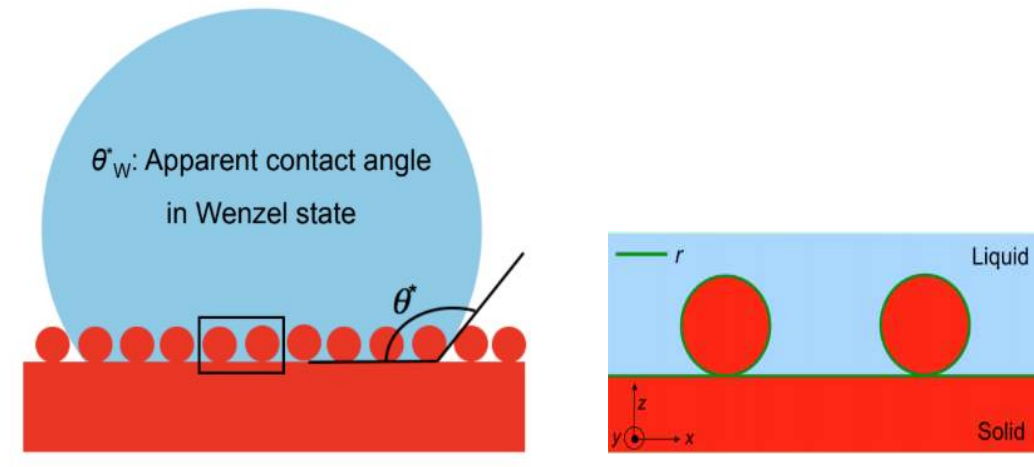


Figure 4. Schematic illustrating apparent contact angle of liquid droplet ( $\theta^*$ ) in Wenzel state (Image reproduced from Dr. Kota's lectures).

As opposed to Wenzel state, in the Cassie Baxter state, the droplet does not penetrate into the texture due to pockets of air trapped between the surface and the liquid droplet. In Cassie state the apparent contact angles are determined by using the relation<sup>18</sup>:

$$\cos\theta^* = f_{sl}\cos\theta + f_{lv}\cos(\pi) = f_{sl}\cos\theta - f_{lv} \quad (5)$$

Where  $f_{lv}$  is the area fraction of liquid-vapour interface and  $f_{sl}$  is the area fraction of solid-liquid interface. From the relation it is clear that lower the  $f_{sl}$ , higher the apparent contact angles which would result in low contact angle hysteresis.

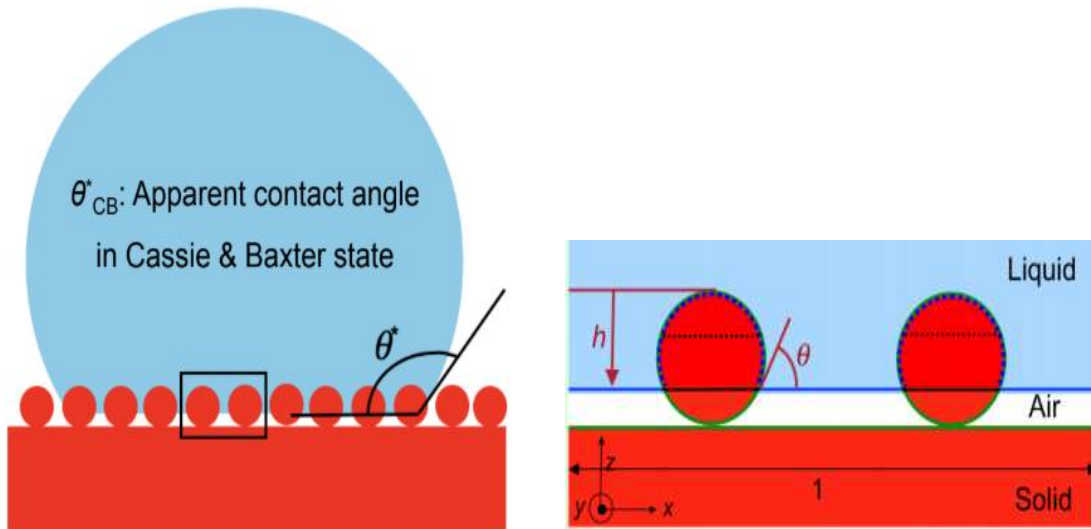


Figure 5. Schematic illustrating apparent contact angle of liquid droplet ( $\theta^*$ ) in Cassie-Baxter state (Image reproduced from Dr. Kota's lectures).

### 1.5 Super Repellent Surfaces and the need for Re-entrant texture

Super repellent surfaces display high apparent contact angles and low contact angle hysteresis and can be classified into superhydrophobic and superoleophobic surfaces<sup>15</sup>. Superhydrophobic surfaces display high apparent contact angles ( $\theta^* > 150^\circ$ ) and low contact angle hysteresis ( $\Delta \theta < 5^\circ$ ) for high surface tension liquids<sup>7,15,19-21</sup>. However, these surfaces cannot repel low surface tension liquids such as oils<sup>15</sup>. Surfaces which display high apparent contact angles ( $\theta^* > 150^\circ$ ) and low contact angle hysteresis ( $\Delta \theta < 5^\circ$ ) for low surface tension liquids are termed as superoleophobic surfaces<sup>22</sup>. Superoleophobic surfaces tend to repel both high and low surface tension liquids<sup>6,22</sup>. Hence a surface that is superoleophobic is superhydrophobic in nature. The

surfaces which can repel both high and low surface tension liquids are termed as superomniphobic surfaces<sup>6,9-11</sup>.

Super repellent surfaces prefer Cassie Baxter state of wetting, however not all textures lead to Cassie Baxter state with low surface tension liquids<sup>15</sup>. This is where role of re-entrant texture is critical to repel low surface tension liquids<sup>23</sup>. High surface tension liquids that display  $\theta > 90^\circ$  can be in a stable Cassie Baxter state with the local texture angle  $\varphi > 90^\circ$ , however this is not the same condition for low surface tension liquids. Low surface tension liquids that display  $\theta < 90^\circ$  can be in a stable Cassie Baxter state if the local texture angle  $\varphi < 90^\circ$ . Hence re-entrant textures is a required condition for superoleophobicity. Such textures with local texture angle  $\varphi < 90^\circ$  are termed as re-entrant textures<sup>15</sup>.

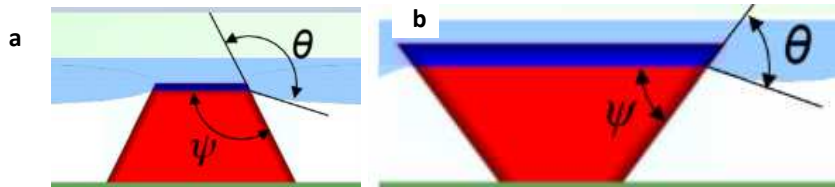


Figure 6. Schematic illustrating a) liquid droplet on a textured surface with texture angle  $>90^\circ$  for  $\Theta > 90^\circ$  in Cassie state. b) liquid drop on a textured surface with texture angle  $<90^\circ$  (re-entrant texture) for  $\Theta < 90^\circ$  in Cassie state (Image reproduced from Dr. Kota's lectures).

## CHAPTER 2

### Dual Superlyophobic Surfaces with Recyclable Polymer

#### 2.1 Introduction

Over the years, surface interaction with liquids have gained a lot of attention that enables us to control wetting properties<sup>24</sup>. As mentioned, surface wettability has led to development of super repellent surfaces which find many commercial and military applications. While all these surfaces find applications in air, there have been very few advances to show surfaces that are super repellent in a fluid medium. Surface interactions with fluids also enables us to control wetting properties inside a fluid medium, where the fluid medium can be either water or oil<sup>25-27</sup>. It is crucial to study wetting properties inside a fluid medium since it finds applications in marine antifouling, oil-water separation and droplet based microfluidic devices<sup>28-31</sup>. Recent times, there has been advances in development of such surfaces to show extreme repellency to low and high surface tension liquids in a liquid medium.

In oil-water systems, the underwater oil contact angle and under-oil water contact angle is a sum of  $180^\circ$  as they supplement each other<sup>32</sup>. Hence a surface that is oleophobic underwater is hydrophilic under-oil and a surface that is hydrophobic under-oil is oleophilic underwater, which is true for a surface which does not display both extremities that is underwater superoleophobicity and under-oil superhydrophobicity<sup>24</sup>. The fabrication of surfaces displaying both underwater superoleophobicity and underoil superhydrophobicity is inspired by “Lotus Effect” and “Fish Scale Effect”<sup>33,34</sup>. Lotus leaves containing hierarchical nano structures can repel high surface tension liquids like water easily. Under an oil medium, the lotus effect is useful to repel water droplets as such surfaces demand re-entrant textures with low surface energy. Such surfaces are termed as underoil superhydrophobic surfaces<sup>25,26</sup>. In a similar way, the fish scale effect is used to repel low surface tension droplets underwater. Such surfaces demand re-entrant textures with high surface

energy and are termed as underwater superhydrophobic surfaces<sup>25,26</sup>. Surface energy plays a crucial role as surfaces with high surface energy have stronger affinity towards water and surfaces with lower surface energy have stronger affinity towards oils<sup>20,32,35</sup>. Therefore, it is counter intuitive for the same surfaces to show both these properties. Surfaces that display both the properties on a same surface are termed as superlyophobic surfaces. The surfaces need to meet two main design criteria in order to display dual superlyophobicity, one the microstructures need to be readily filled by water and oil without air being trapped when immersed in either water or oil, second the submerged microstructures should support steady oil-water interface when second liquid is introduced, that is the trapped liquid film is not displaced by the suspended liquid<sup>20</sup>. These two design criteria's is satisfied if the microstructures possess re-entrant texture which is a necessary condition for preparing dual superlyophobic surfaces. And as mentioned surface energy is another key parameter that plays a key role in fabricating these surfaces.

Prior reports have shown fabrication of such superlyophobic surfaces<sup>36,37</sup>. However, to our knowledge the surfaces reported involve complex fabrication processes, expensive reagents and non-recyclable materials. In this work we have designed dual superlyophobic surfaces with recently discovered recyclable polymer by combining re-entrant texture and appropriate surface energy. We fabricated these surfaces using a simple spray coating method that resulted in textured surfaces with re-entrant structures. The surface energy of the textured surfaces was then modified through plasma treatment. Our surfaces display under-water superoleophobicity for low surface tension liquids like oils and under-oil superhydrophobicity for high surface tension liquids like water. We envision that our dual superlyophobic surfaces will find applications in membrane separation, antifouling coatings and droplet-based fluidic devices. To show potential practical applications we demonstrated manipulation of ferrofluid droplets under liquid and effective oil-water separation with efficiency greater than 99%.

## 2.2 Materials

The recently discovered recyclable polymer was taken from Eugene Chen's group at Colorado State University. Dichloromethane used as a solvent to dissolve the recyclable polymer was purchased from Gelest. The spray coater was purchased from Paasche to spray coat the dual superlyophobic surfaces. Plasma etcher was used to hydroxylate the surface with oxygen plasma. The scanning electron microscope (SEM) was used to characterize surface morphology of the surfaces. The wettability of the surfaces was determined by measuring the static contact angles, apparent contact angles and roll off angles using a Ramé-Hart 260F4 goniometer. Different low surface tension liquids were purchased from Gelest. The ferrofluid used for manipulation of under liquid droplets was purchased from Gelest. Aluminium porous meshes was used as a substrate to demonstrate oil-water separation.

## 2.3 Methods

### *2.3.1 Fabrication of Dual Superlyophobic Surfaces*

Figure 7 shows the schematic illustrating the fabrication of dual superlyophobic surfaces using recyclable polymer. 2.5g of the recyclable polymer was first dissolved in 20mL dichloromethane in a glass vial. The polymer was completely dissolved by heating the glass vial at 70°C on a hot plate and shaking every 20 mins. The solution was then spray coated on a glass slide with the help of a spray coater at 30 psi pressure kept at a distance of 30cm from the head of the spray gun. The surface energy of the resulting spray coated surfaces was modified by exposing the surfaces to oxygen plasma for 20 sec to form dual superlyophobic surfaces.

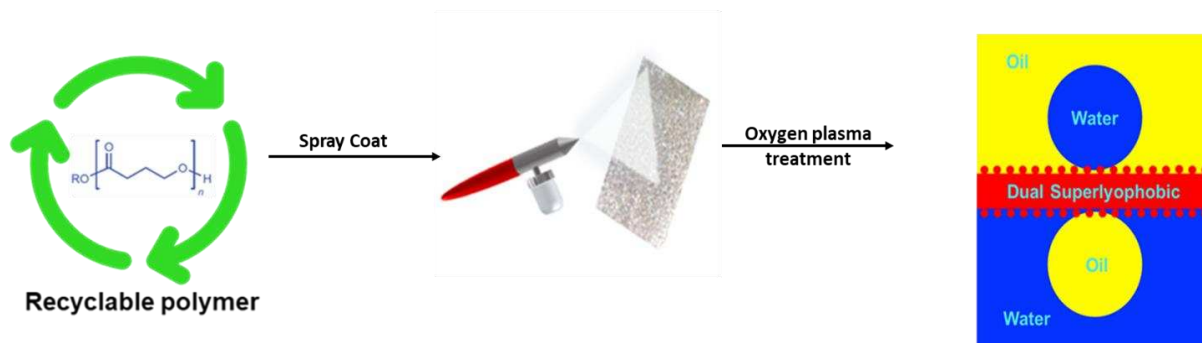


Figure 7. Schematic illustrating the fabrication of Dual Superlyophobic surfaces.

### 2.3.2 Surface characterization of Dual Superlyophobic surfaces

The morphology of the surfaces was determined using a JOEL 6500 F scanning electron microscope (SEM) at a voltage of 15 kV.

### 2.3.3 Surface Wettability of Dual Superlyophobic surfaces

The wettability of the dual superlyophobic surfaces was characterized by measuring the static contact angles, apparent contact angles and roll off angles on a goniometer (Ramé-Hart 260F4). The static contact angles, apparent contact angles and the sliding angles were measured with a 20  $\mu$ L water droplet. The error in measurement of static contact angles, apparent contact angles and roll off angles were  $\pm 3^\circ$ ,  $\pm 3^\circ$  and  $\pm 1^\circ$  respectively.

### 2.3.4 Surface Energy of the recyclable polymer

The surface energy was determined on smooth surfaces coated with recyclable polymer. The recyclable polymer was spin coated at 1500 rpm for 75 sec to form a smooth coating. The advancing contact angles of a polar liquid and a non-polar liquid was measured to determine the surface energy. The surface energy was estimated by using the Owen Wendt relation<sup>38</sup>.

## 2.4 Results and Discussions

The SEM images (Figure 8a) indicated the formation of cylindrical fibers with re-entrant textures upon spray coating. The spray coated surfaces displayed an apparent contact angle of  $130^\circ$  in air. The surface energy of these surfaces were further tuned to display underwater superoleophobicity and under-oil superhydrophobicity. The spray coated surfaces were hydroxylated by exposing them to oxygen plasma for 20 sec. The surface energy of the recyclable polymer was found to be  $26.60 \text{ mJ/m}^2$ . Upon hydroxylation the surface energy was found to be  $58 \text{ mJ/m}^2$ . The surfaces after hydroxylation were hydrophilic (Figure 8b) and superoleophilic in air (Figure 8c). These surfaces after hydroxylation were used to characterize wettability for dual superlyophobicity (i.e., display both underwater superoleophobicity and under-oil superhydrophobicity).

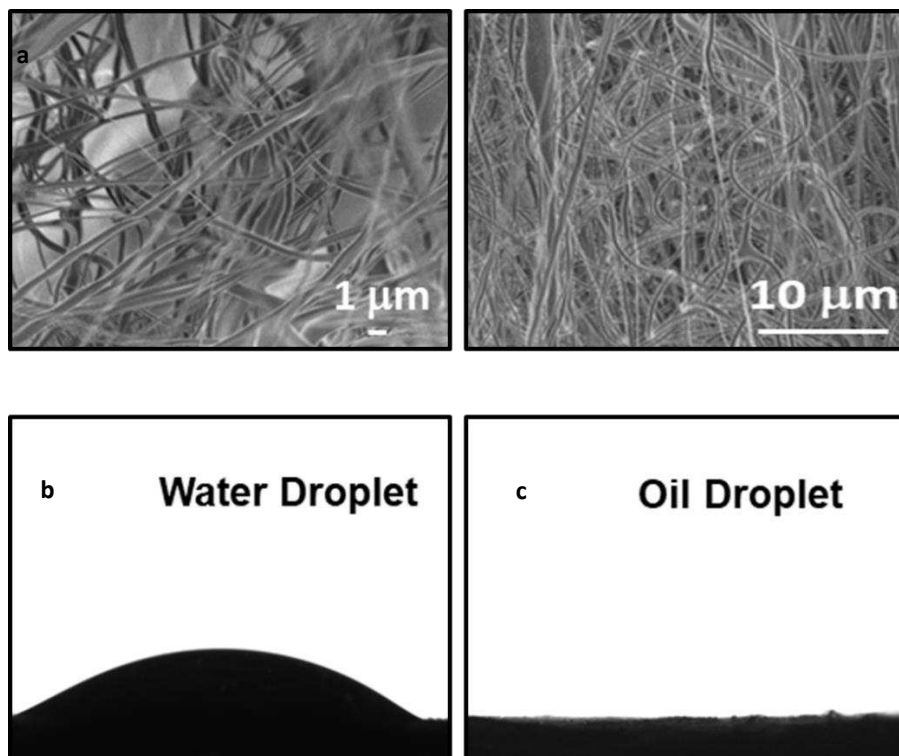


*Figure 8. a) SEM images of the dual superlyophobic surfaces b) Static contact angle of a water droplet (hydrophilic) in air on dual superlyophobic surface c) Static contact angle of a hexadecane droplet (superoleophilic) in air on dual superlyophobic surface.*

To characterize dual superlyophobicity, the surfaces were first analyzed for underwater superoleophobicity. The hydroxylated surfaces were pre wetted with water to characterize underwater superoleophobicity on smooth and textured surfaces. Different low surface tension liquids of varying surface tensions were used to characterize underwater superoleophobicity namely krytox, hexadecane, tetradecane rapeseed oil and silicone oil. The results indicated underwater oleophobicity on smooth surfaces whereas the textured surfaces displayed underwater superoleophobicity (Figure 9a and 9b respectively). The apparent contact angles were measured on the textured surfaces and were found to be  $> 150^\circ$  for all the low surface tension liquids. The contact angles on the smooth surfaces were  $< 120^\circ$  for all the low surface tension liquids. The roll off angles were determined on smooth and textured surfaces. The results indicated low roll off angle for low surface tension liquid (krytox) on the textured surfaces indicating low hysteresis on the textured surfaces (Figure 9c). The droplets however on the smooth surfaces could not roll off at a higher tilt angle indicating the need for textured surfaces with re-entrant texture for underwater superoleophobicity. Hence the surfaces displayed high apparent contact angles and low roll off angles for low surface tension liquids (Figure 10).

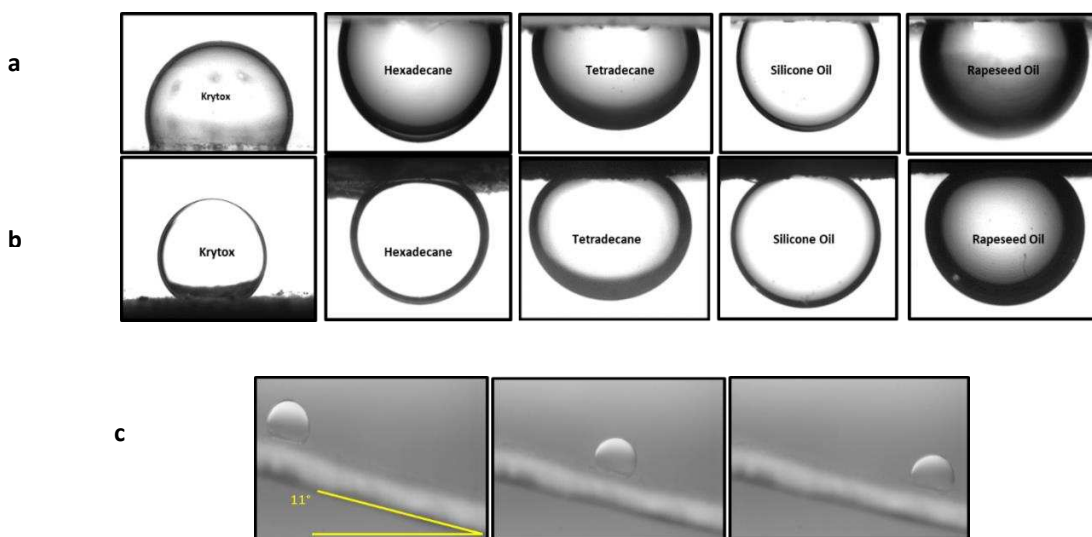


*Figure 9. a) Underwater oleophobicity of various low surface tension liquids on smooth surfaces b) Underwater superoleophobicity of various low surface tension liquids on textured surfaces c) Roll off angle of a krytox droplet underwater.*

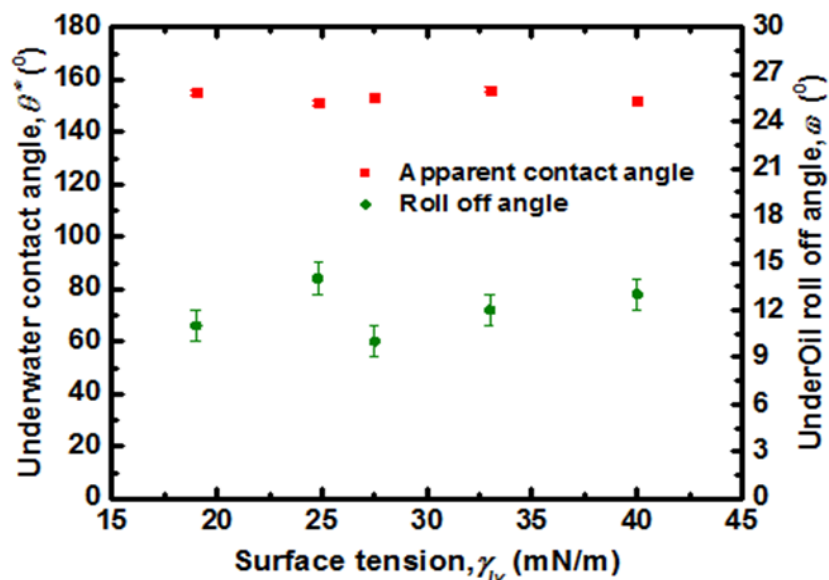


Figure 10. Underwater apparent contact angles and roll off angles of all low surface tension liquids.

The wettability of the surfaces were further characterized for underoil superhydrophobicity on smooth and textured surfaces. Water and ethanol mixtures were used to characterize underoil superhydrophobicity. The results indicated underoil hydrophobicity on smooth surfaces whereas the textured surfaces displayed underoil superhydrophobicity (Figure 11a and 11b respectively). The apparent contact angles were measured on the textured surfaces and were found to be  $> 155^\circ$  for water and ethanol mixtures. The contact angles however on the smooth surfaces were  $< 130^\circ$  for water and ethanol mixtures. The results indicated low roll off angles for water and ethanol mixtures on the textured surfaces indicating low hysteresis on the surfaces (Figure 11c). The droplets however on the smooth surfaces could not roll off at a higher tilt angles indicating the need for textured surfaces with re-entrant textures for underoil superhydrophobicity. Hence the surfaces displayed high apparent contact angles and low roll off angles for water and water-ethanol mixtures liquids (Figure 12).

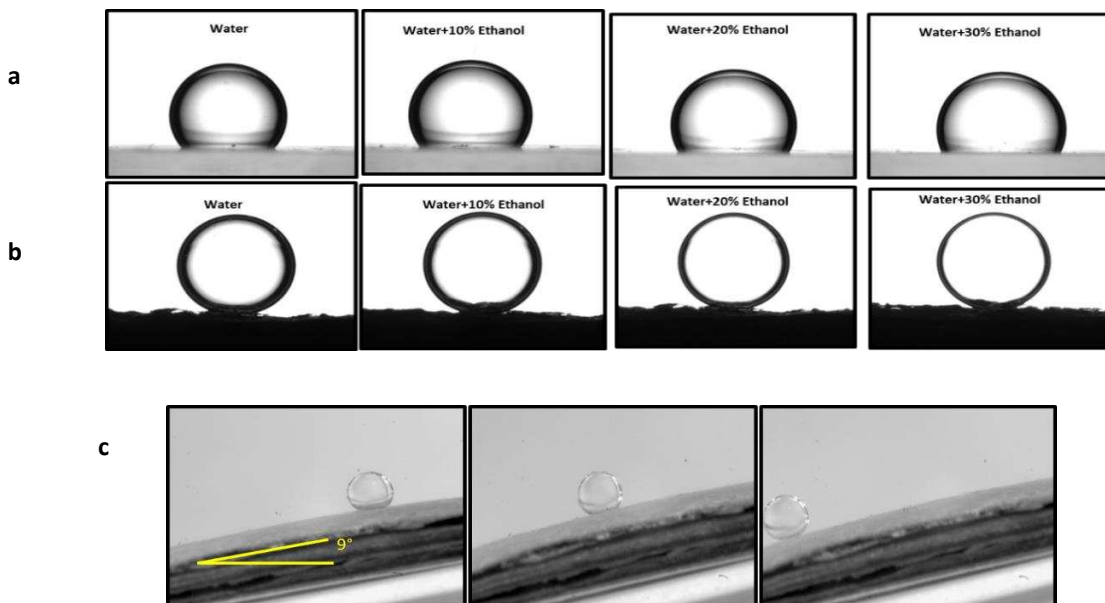


Figure 11. a) Under-oil hydrophobicity of various water-ethanol mixtures on smooth surfaces b) Under-oil superhydrophobicity of various water-ethanol mixtures on textured surfaces c) Roll off angle of a water droplet under-oil.

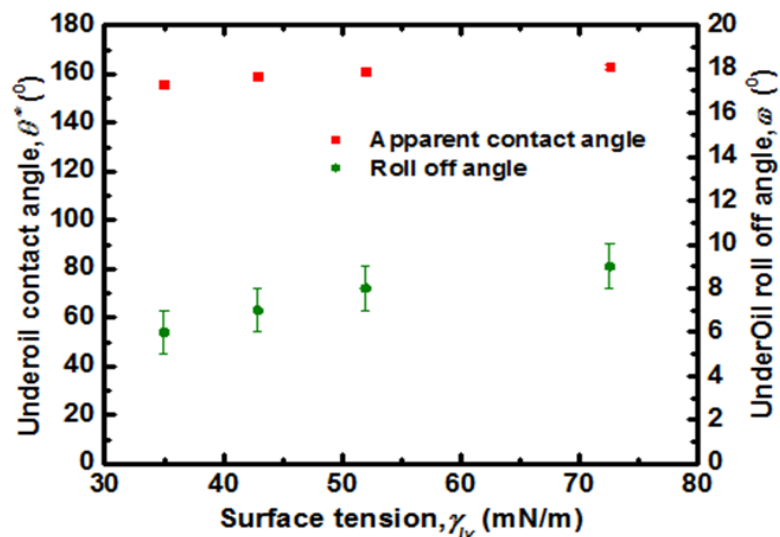


Figure 12. Underoil apparent contact angles and roll off angles for water and water-ethanol mixtures.

The surfaces hence display dual superlyophobic properties (underwater superoleophobicity and underoil superhydrophobicity). The robustness factor  $A^*$  was also determined on the dual superlyophobic surfaces which is a measure of breakthrough pressure and reference pressure.

$A^*$  is defined as the ratio of breakthrough pressure ( $P_{\text{breakthrough}}$ ) to reference pressure, where reference pressure is given by  $P_{\text{ref}} = 2\gamma_{lv}/l_{\text{cap}}^6$ . For  $A^* \ll 1$ , the contacting liquid cannot maintain a composite interface whereas for  $A^* \gg 1$ , the contacting liquid maintains a composite interface which in turn can withstand high breakthrough pressures<sup>1,15</sup>. For cylindrical textures the robustness factor  $A^*$  is given by  $A^*_{\text{cylinder}} = P_{\text{breakthrough}}/P_{\text{ref}} = l_{\text{cap}} (1 - \cos\Theta) / R (D^*_{\text{cylinder}} - 1) (D^*_{\text{cylinder}} - 1 + 2\sin\Theta)$ <sup>1</sup>. In both the cases that is underwater and under-oil, the  $A^* \gg 1$  hence proving that the contacting liquid maintains a stable composite interface withstanding high breakthrough pressures.

## 2.5 Applications

To show potential applications, these surfaces were tested for oil-water separation and manipulation of ferrofluid droplets.

### *2.5.1 Manipulation of underwater ferrofluid droplets*

Manipulation of aqueous droplets finds various applications in microfluidics, cell sorting and biochemical analysis<sup>39</sup>. Manipulation of droplets can be classified into active methods which involve external fields such as a magnetic field, electro wetting etc., and passive methods which involve surface morphology such as Laplace pressure gradient and surface wettability to manipulate droplets<sup>40</sup>. Manipulation of droplets via magnetic field finds many advantages over other methods. Ferrofluids are colloidal suspensions which contain magnetic nanoparticles in them<sup>41</sup>. They are coated with surfactants, where in the carrier fluid can be either water or oil<sup>41</sup>. These fluids find many commercial applications in lubrication, vacuum, sensors, and dampers. Ferrofluids have been used in microfluidics to actuate droplets under the influence of external magnetic fields. Droplet based microfluidics result in droplet mixing, separation, transport etc., which enhances control over individual droplets<sup>42</sup>. There have been many on demand manipulation of ferrofluidic droplets on various surfaces that have been shown using surface

modification techniques, varying geometries<sup>43</sup>. While there have been reports showing manipulation of ferrofluidic droplets (shape evolution and splitting of droplets) in air on hydrophobic surfaces<sup>44,45</sup>, as per our knowledge there are very few works reported showing manipulation of ferrofluidic droplets under a liquid medium. Here in we report manipulation of ferrofluidic droplets underwater where we show movement and splitting of ferrofluidic droplets under the influence of an external magnetic field. The manipulation of ferrofluid droplets was characterized underwater using an oil based ferrofluid. An oil based ferrofluid of volume 50 $\mu$ L was placed on the dual superlyophobic surface and its motion was controlled externally by moving the magnet below it, where the magnetic field is applied in the direction perpendicular to the droplet. The oil droplet tends to bead up on these surfaces like a sphere as indicated in Figure 13a.

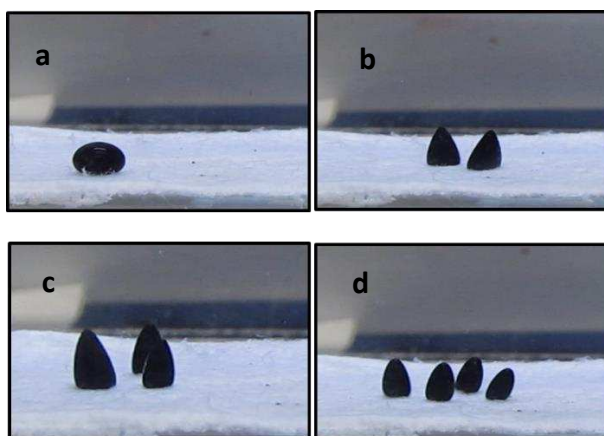


*Figure 13. a) Oil based ferro fluid on the dual superlyophobic surface underwater. b, c, d) Figure indicating the motion and splitting of ferro fluid on the dual superlyophobic surface with external magnetic field.*

As the magnet is brought closer to the substrate the ferrofluid tends to split into spikes as indicated in the Figure 13b. With the increase in the magnetic flux, that is when the magnet is moved towards the substrate the apparent contact angle of the droplet reduced eventually and at a point splits into multiple droplets as shown in Figure 13c and 13d. These spikes continue to

bead on the surface and move on the surface effortlessly with the influence of the external magnet. On decreasing the magnetic field by moving the magnet away from the substrate the droplets tend to get back to its original spherical shape. The complete motion and splitting of droplet was achieved indicating the robustness of these dual superlyophobic surfaces.

### *2.5.2 Oil/water Separation*

The field of oil-water separation plays a significant role in resolving potential industrial concerns over oil-water pollution<sup>1-3</sup>. It is in fact a challenge to remove toxic contaminants with high efficiency and low energy consumption. As of today, there have been many novel materials that have been reported to tackle such problems. Recent studies have shown development of materials and meshes which possess super wetting properties as a medium for effective oil-water separation<sup>46-48</sup>. However, fabrication of these membranes for effective oil-water separation have been reported using complex fabrication techniques, expensive reagents and instruments. Some reports show effective oil-water separation using external stimulation like temperature, light irradiation and pH induced. Hence there is a need for developing membranes with simpler techniques and low time and energy consumption. The oil-water separation on the dual superlyophobic surfaces was characterized by separating oil from water and water from oil. Thin porous aluminium meshes were used to demonstrate oil-water separation. The recyclable polymer was spray coated on these meshes and the surface energy was tuned by hydroxylating the meshes with oxygen plasma for 20 sec. The spray coated meshes were used for effective oil-water separation. We used wettability properties to separate oil or water from oil/water mixture with respect to density of water being heavier than oil or not. For separation of water from oil, the mesh was first pre wetted with water, the red coloured liquid chosen for this demo was hexadecane (red colour) whose density is less than water (blue coloured liquid) as shown in Figure 14a-c. During oil/water separation hexadecane remained stable on the pre wetted mesh while water permeates and is separated out. Similarly, to separate oil from water, the meshes were pre wetted with oil after

oxygen plasma treatment for 20 sec. The oil chosen for this demo was krytox which is shown as a colourless liquid whose density is greater than water which is shown as a blue coloured liquid in Fig 14d-f.

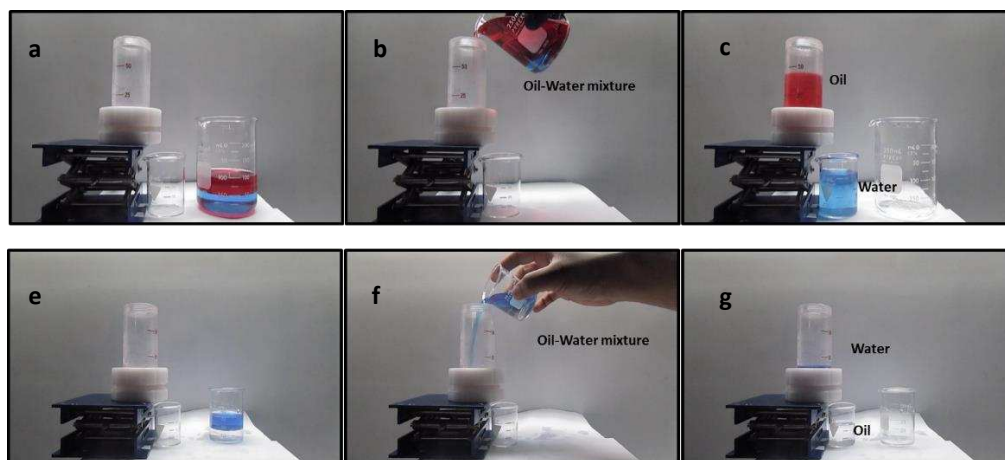


*Figure 14. a-c) Separation of water from hexadecane-water mixture using dual superlyophobic membrane. e-f) Separation of krytox from krytox-water mixture using dual superlyophobic membrane.*

During oil/water separation water remained stable on the oil pre wetted mesh while oil (krytox 101) permeates through and was separated out. The driving force was the gravity under which the separation of oil-water mixture took place, where in both the cases the lighter liquid stayed on top of the membrane and the heavier liquid was separated out. The separation efficiency was calculated using the relation  $\eta = (m_1/m_0)$  where  $m_0$  and  $m_1$  are the mass of rejected liquid phase before and after separation process respectively<sup>49</sup>. The separation efficiency in both the cases was calculated and was found to be 99%. The experiment was carried out for 5 measurement cycles and the separation efficiency remained the same.

## CHAPTER 3

### **PEGylated hydrophilic slippery surfaces for low protein adsorption, platelet adhesion and activation and bacterial adhesion**

#### 3.1 Introduction

Over the years, there has been vast development in materials for blood contacting implantable devices where in the prime area of interest was to reduce protein adsorption, platelet adhesion and activation and bacterial adhesion<sup>9,50,51,52</sup>. When a biocompatible material encounters blood, fibrinogen gets adsorbed onto the surface which forms the basis for coagulation cascade<sup>4,5</sup>. The adsorbed fibrinogen further instigate platelet, leukocyte and bacterial adhesion which leads to problems related to blood clotting thrombosis leading to the failure of the device<sup>4</sup>. The adsorbed proteins also lead to the formation of factor XII which results in thrombin formation which then mediates conversion of fibrinogen to a fibrin mesh which traps the red blood cells to form thrombosis<sup>53</sup>. To prevent all these events, medical professionals prescribe anti-coagulants and blood thinners such as Aspirin, Clopidogrel and Vorapaxar to patients for rest of their life<sup>54,55</sup>, which have their own long-term negative effects such as internal bleeding, nosebleeds, weakened immune response etc. which affects the overall health of the patients. Further bacterial adhesion on surfaces lead to the formation of biofilms which enhance the growth of bacteria colonies<sup>56,57</sup>. The biofilm contains proteins and polysaccharides developed by bacteria which protects them from antibiotics<sup>20</sup>. Bacterial adhesion is a serious issue especially with blood contacting medical devices<sup>58,5</sup>. Bacterial adhesion cause heart valve infections, catheter biofilm infections and blood stream infections<sup>57</sup>. The inhibition of bacterial infections on surfaces is crucial to reduce medical device failures<sup>59</sup>. Hence it is important to study blood-material and bacteria-material interactions to understand the underlying mechanisms which lead to better design of blood contacting materials.

Titanium and its alloys in general have been extensively used for blood contacting implantable devices such as stents, heart valves due to their excellent mechanical properties such as high corrosion resistance, osseointegration capabilities and high specific strength<sup>4,60,61</sup>. But titanium and its alloys can have negative effects when they encounter blood and proteins<sup>62,63</sup>. It is well known that over the years, there has been extensive research on surface modification of these bio compatible materials to prevent blood clotting<sup>64,65</sup>. One such strategy is to modify the surface chemistry of the surfaces with functional groups such as -CH<sub>3</sub>, -NH<sub>2</sub>, -COOH etc. By tailoring the functional groups, the surface energy and wettability of the surfaces can be altered which can affect proteins and cell interactions<sup>66,67</sup>. Another strategy is employing superhydrophobic surfaces to improve hemocompatibility is to reduce platelet adhesion/activation and protein adsorption on the surfaces<sup>68,69</sup>. These surfaces with varied topography, roughness and wettability along with surface modification with a low surface energy silane show a significant amount of reduced platelet adhesion/activation and protein adsorption due to the overall reduction in the material-blood interfacial area which in turn lead to reduction in the amount of proteins adsorbed, thus reducing platelet adhesion/activation and bacterial adhesion<sup>70</sup>. However, the major concern is the stability of these surfaces over time when exposed to blood, questioning the robustness of these surfaces. Hence there is a need to develop robust surfaces which can reduce protein adsorption, platelet adhesion and activation and bacterial adhesion for longer durations.

Though superhemophobic bio compatible materials (displaying contact angles > 150° and low roll off angles <10°) are commonly researched and developed to prevent adverse effects caused when it encounters blood<sup>9</sup>, as far as we know there has been lesser development in hydrophilic repellent surfaces for blood contacting devices. Hydrophilic surfaces typically have low contact angles (<90°) and show lower affinity to adsorb proteins on the surfaces<sup>71,72</sup>. In literature, hydrophilic surfaces have been developed by covalently bonding polyethylene glycol (PEG) on to the surfaces<sup>73-75</sup>. However, results have not shown a significant reduction in platelet

adhesion/activation and bacterial adhesion on PEGylated surfaces<sup>76</sup>. In this study, we have developed polyethylene glycol based hydrophilic slippery surfaces by covalently attaching PEG silane via O-Si bonds to hydroxylated surface to form PEG brushes. The hydrophilic slippery surfaces formed are chemically homogeneous with low molecular weight PEG brushes with high grafting density. These surfaces can easily repel high surface tension liquids like water and blood with a tilt angle of  $<10^\circ$ . It is envisioned that these surfaces can be effectively used to reduce protein adsorption, platelet adhesion/activation and bacterial adhesion and the use of slippery surfaces can be an ideal approach for designing surfaces for blood-contacting medical devices.

## 3.2 Methods

### *3.2.1 Fabrication of PEGylated hydrophilic slippery surfaces*

Schematic (Figure 15) illustrates the fabrication of PEGylated hydrophilic slippery surfaces. Commercially available single side polished (SSP) silicon wafers with thickness of 650 $\mu$ m were used as substrates in this study. The silicon wafers were cut into 5 cm X 3 cm pieces with metal cutter and ultrasonically cleaned with acetone, ethanol and DI water separately for 10 mins each. The surface were subsequently air-dried using nitrogen. The pre-cleaned wafers were then subjected to O<sub>2</sub> plasma at 10 psi in 10cm<sup>3</sup>/min of oxygen gas for 15 mins. The hydroxylated silicon wafer surfaces were dip coated in a solution of 3 $\mu$ L PEG silane (2 – [Methoxy (Polyenthleneoxy) 6-9 propyl] Trimethoxysilane), 12  $\mu$ L HCl and 40 mL toluene for 9 hrs. The silicon wafers were rinsed with DI water to remove excess PEG silane present on the surface and were subsequently air-dried using nitrogen. The surfaces were rinsed three times with sterile phosphate buffer solution (PBS) prior to all biological studies.

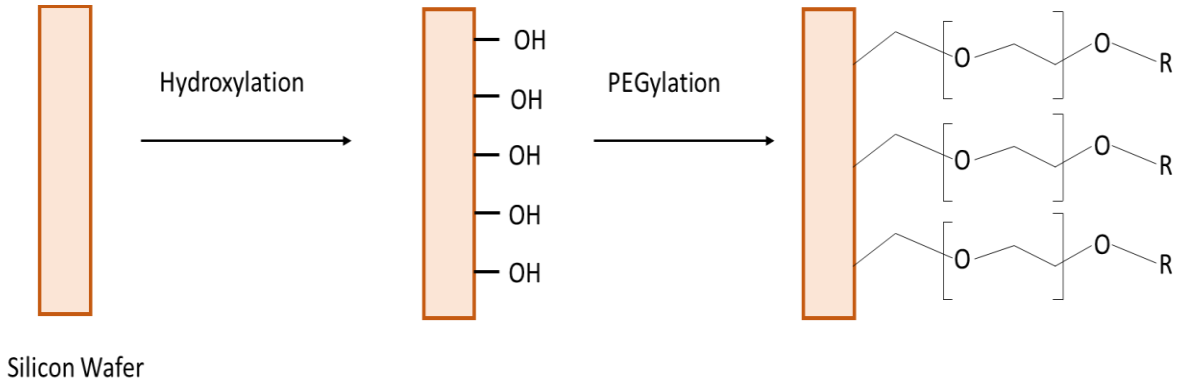


Figure 15. Schematic illustrating the fabrication of PEGylated hydrophilic slippery surfaces where R represents methyl groups.

### 3.2.2 Surface characterization of PEGylated hydrophilic slippery surfaces

The wettability of the surfaces was determined by measuring the static contact angles using a goniometer (Ramé-Hart 260F4). The static contact angles were measured on three different spots on the surface with a 20  $\mu$ L water droplet. The droplet was pipetted on the surface and was allowed to sit for 10 sec before the static contact angles were measured. The error in the contact angles measured were  $\pm 2^\circ$ . The advancing (maximum) and receding (minimum) contact angles were determined to estimate the contact angle hysteresis on the surfaces. The solid surface energy was estimated by measuring the advancing (maximum) contact angles of a polar liquid and a non-polar liquid. The dispersive and polar components of the solid surface energy were estimated using Young's (Eq 6) and Owen Wendt relationship<sup>38</sup> (Eq 7):

$$\gamma_{lv} \cos\theta = \gamma_{sv} - \gamma_{sl} \quad (6)$$

$$\gamma_{sl} = \gamma_{sv} + \gamma_{lv} - 2(\sqrt{\gamma_{sv}^d \gamma_{lv}^d} + \sqrt{\gamma_{sv}^p \gamma_{lv}^p}) \quad (7)$$

where  $\gamma_{lv}$  is the liquid interfacial tension,  $\gamma_{lv}^p$  and  $\gamma_{lv}^d$  are its polar and dispersive components,  $\gamma_{sl}$  is the solid liquid interfacial energy and  $\gamma_{sv}$  is the solid surface energy.  $\gamma_{sv}^p$  and  $\gamma_{sv}^d$  are polar and

dispersive components of the solid surface energy and  $\theta$  is the advancing contact angle for a liquid drop. The overall surface energy is the sum of polar and dispersive components (Eq3).

$$\gamma_{sv} = \gamma_{sv}^d + \gamma_{sv}^p \quad (8)$$

The chemistry of different surfaces was characterized by PE-5800 X-ray photoelectron spectroscopy. Survey spectra scans were collected from 0 to 1100 eV with a pass energy of 187.85 eV. High resolution scans were collected for carbon (C1s) using a pass energy of 10eV. Surface elemental composition of the surfaces was estimated using peak fit analysis in the origin software.

### *3.2.3 Protein adsorption on PEGylated hydrophilic slippery surfaces*

Protein adsorption was characterized on different surfaces using a micro-BCA assay. The surfaces were incubated with 300  $\mu$ L of 0.1mg/mL of protein solution (albumin or fibrinogen) in PBS, in a 48-well plate on a horizontal shaker at 100 rpm, 37°C and 5% CO<sub>2</sub> for 2hrs. After incubation period, the protein solution was aspirated, the surfaces were transferred to a new 48-well plate and rinsed three times with PBS and. Subsequently, the surfaces were incubated with 300  $\mu$ L of 1 % sodium dodecyl sulphate (SDS) on a horizontal shaker at 100 rpm, 37°C and 5% CO<sub>2</sub> for 4 hrs. The surface exposed SDS was incubated with equal volume of working reagent (prepared as directed by micro-BCA assay instructions) at 100 rpm, 37°C and 5% CO<sub>2</sub> for 2 hrs. The absorbance of the resulting solution was measured at a wavelength of 562nm using a plate reader. A standard curve with known protein concentrations was plotted by following the micro-BCA assay instructions and was used to convert the absorbance of resulting solution to protein concentrations.

### *3.2.4 Isolation of Platelet rich plasma (PRP) from whole human blood*

Whole human blood was drawn from healthy donors. The protocol was approved by Colorado State University Institutional Review Board and was performed in compliance with National Institute of Health's Guiding Principle for Ethical Research. The blood was drawn into 6 mL tubes coated with anticoagulant ethylenediaminetetraacetic acid (EDTA). The first tube was discarded to avoid the platelet plug and locally activated platelets as a result of needle insertion. The PRP was separated from the blood by centrifuging the tubes at 150g for 15 mins. The tubes were let to sit for 15 mins after centrifugation and the PRP was used for cell studies on different surfaces.

### *3.2.5 Cytotoxicity on PEGylated hydrophilic surfaces*

Cytotoxicity was evaluated on different surfaces by using Lacate dehydrogenase (LDH) assay kit. The surfaces along with positive control (provided with the assay) and negative control (PRP treated with Triton-X provided with the assay) were incubated in a 48-well plate with 400  $\mu$ L of PRP on a horizontal shaker at 100 rpm, 37°C and 5% CO<sub>2</sub> for 2 hrs. 100  $\mu$ L of surface-exposed PRP was pipetted to the 96-well plate and protocol provided by the manufacturer was followed. The absorbance of the resulting solution was measured at a wavelength of 490 nm using a plate reader.

### *3.2.6 Cell adhesion on PEGylated hydrophilic slippery surfaces*

Cell adhesion was evaluated on surfaces by staining the live cells with Calcein-AM stain and imaging them using fluorescence microscopy. The surfaces were incubated in a 48-well plate with 400  $\mu$ L of PRP on a horizontal shaker at 100 rpm, 37° C and 5% CO<sub>2</sub> for 2 hrs. After incubation, PRP was aspirated and the surfaces were rinsed three times with PBS to remove any unadhered cells. The surfaces were then stained using 300  $\mu$ L of 5% Calcein-AM solution in PBS for 20 mins at room temperature in a dark environment. The stain solution was then aspirated, and the

surfaces were rinsed two times with PBS to remove any excess stain solution. The surfaces were imaged using the Zeiss Axivision fluorescence microscope. The images were further processed using ImageJ software to estimate the percentage area of live cell adhesion on the surfaces.

### *3.2.7 Identification of platelets and leukocytes adhered on PEGylated hydrophilic slippery surfaces*

The platelets and leukocytes adhered on different surfaces were identified by staining the adhered cells using DAPI (4, 6 – diamidino – 2 – phenylindole) and Rhodamine Phalloidin and imaging them using fluorescence microscope. The surfaces were incubated in a 48-well plate with 400  $\mu$ L of PRP on a horizontal shaker at 100 rpm, 37° C and 5% CO<sub>2</sub> for 2 hrs. After incubation, PRP was aspirated and the surfaces were rinsed three times with PBS to remove any unadhered cells. This was followed by fixing the cells by incubating them in 3.7 % formaldehyde solution for 15 mins. The surfaces were rinsed three times with PBS and incubated in a solution of 1% Triton X for 3 mins. The surfaces were further rinsed three times with PBS and transferred to a new 48-well plate. Subsequently, the surfaces were incubated with 300  $\mu$ L of 0.05% Rhodamine Phalloidin solution (8ml PBS with 40  $\mu$ L working Rhodamine solution) for 20 mins. Later, the samples were incubated with 21  $\mu$ L of 3% DAPI stain stock solution for 5 mins. The surfaces were rinsed two times with PBS and imaged using the fluorescence microscopy. The images were further processed using ImageJ software to estimate the percentage area of platelets and leukocytes adhered on the surfaces.

### *3.2.8 Platelet activation on PEGylated hydrophilic slippery surfaces*

Platelet activation on the surfaces was evaluated using SEM. The surfaces were incubated in a 48-well plate with 400  $\mu$ L of PRP on a horizontal shaker at 100 rpm, 37° C and 5% CO<sub>2</sub> for 2. After incubation, PRP was aspirated and the surfaces were rinsed three times with PBS to remove any unadhered cells. The adhered platelets on different surfaces were fixed by incubating the

surfaces in a primary fixative solution containing 6% glutaraldehyde, 0.1M sodium cacodylate and 0.1M sucrose in DI water for 45 mins. The surfaces were then transferred to a buffer solution containing of 0.1M sodium cacodylate and 0.1M sucrose for 10 mins. Subsequently the surfaces were incubated in 35%, 50%, 70% and 100% ethanol solutions for 10 mins each respectively. The surfaces were air dried and imaged for SEM. The platelet activation on the surfaces was evaluated using a JOEL 6500 F scanning electron microscope at a voltage of 15 kV. The surfaces were sputter coated with 5nm gold coating prior to SEM for high resolution imaging. The surfaces were imaged at 500X and 5000X magnification.

### *3.2.9 Whole human blood clotting on PEGylated hydrophilic slippery surfaces*

The amount of free hemoglobin on the surfaces after exposure to whole blood was evaluated using a plate reader. Lower amount of hemoglobin indicates more blood clotting on the surface. The whole human blood was drawn from a healthy donor in a tube without anticoagulants. 20  $\mu$ L of blood was pipetted on the surfaces immediately and the blood was allowed to clot for 15, 30 and 45 mins. After specific time intervals, 2 mL of DI water was added on each surface and the well plate was placed on a horizontal shaker for 30 secs at 100 rpm and allowed to rest for 5mins. 200  $\mu$ L of this solution was pipetted into a 96 well plate and the absorbance was read using a microplate reader at a wavelength of 540nm. 20  $\mu$ L of whole blood was added to 2mL DI water and the amount of free hemoglobin was measured for positive control with a volume of 200  $\mu$ L in a 96 well plate using a microplate reader at a wavelength of 540nm.

### *3.2.10 Preparation of bacteria culture*

Bacteria (*Staphylococcus Aureus* and *Escherichia Coli*) was incubated in a tryptic soy broth (TSB) medium for 8 hrs at 37°C. The initial concentrations of the bacteria solution were determined using a plate reader at a wavelength of 562 nm. The bacteria solution was diluted for the

absorbance value of 0.52 which equates to bacteria concentration of  $10^9$  (CFU/mL). Further the bacteria solution was diluted to  $10^6$  (CFU/mL) for the study. The surfaces were incubated with 500  $\mu$ L of the bacterial solution for 6 hrs and 24 hrs at 37°C.

### *3.2.11 Anti-bacterial activity on PEGylated hydrophilic slippery surfaces*

Bacterial adhesion on different surfaces was evaluated by using fluorescence microscope and SEM. After incubation with bacteria, the surfaces were stained with 500  $\mu$ L of Live/Dead bacteria stain by combining equal amounts of 20mM propidium iodide and 3.34mM SYTO™ 9 for 15 mins. The surfaces were then rinsed with 500  $\mu$ L PBS for 5 mins. The adhered bacteria on the surfaces were fixed by incubating them in 3.7% formaldehyde solution for 15 mins at room temperature. The formaldehyde solution was aspirated, and the surfaces were rinsed two times with PBS and imaged using the fluorescence microscopy. The images were further processed using ImageJ software to evaluate the percentage area of Live/Dead bacteria on the surfaces.

After incubation, the bacteria on the different surfaces was fixed by placing the samples in a primary fixative solution containing 6% glutaraldehyde, 0.1M sodium cacodylate and 0.1M sucrose in DI water for 45 mins. The surfaces were then transferred to a buffer solution containing of 0.1M sodium cacodylate and 0.1M sucrose for 10 mins. Subsequently the surfaces were incubated in 35%, 50%, 70% and 100% ethanol solutions for 10 mins each respectively. The surfaces were air dried and imaged for SEM. The morphology of the bacterial adhesion on the surfaces was evaluated using a JOEL 6500 F scanning electron microscope at a voltage of 15 kV. The surfaces were sputter coated with 5nm gold coating prior to SEM for high resolution imaging. The surfaces were imaged at 500X and 2500X magnification.

### 3.2.12 Statistical Analysis

SEM and XPS analysis was done on at least three different samples for each surface. Contact angles, sliding angles and contact angle hysteresis was evaluated on at least three different locations on each sample for three different samples for each surface ( $n_{\min} = 9$ ). Protein adsorption on the surfaces was evaluated on at least three different samples for each surface and repeated three times ( $n_{\min} = 9$ ). Fluorescence microscopy, platelet activation and whole blood clotting was repeated three times with three different samples for each surface ( $n_{\min} = 9$ ). The results were quantized statistically using the software JMP Pro. The results were considered to be statistically significant with a p value  $< 0.05$ .

## 3.3 Results and Discussion

The chemistry of different surfaces was characterized by PE-5800 X-ray photoelectron spectroscopy. Survey spectra scans were collected from 0 to 1100 eV with a pass energy of 187.85 eV on the surfaces to determine the surface elemental composition (Figure 16a). The PEGylated and the unmodified surfaces showed peaks for O1s (529-530 eV), C1s (284 eV), Si2s (161.5 eV) and Si2p (100 eV). The PEGylated surfaces showed higher O1s, C1s and Si2p peaks due to the effective grafting of the covalently bonded PEG groups. However, there was a decrease in the silicon concentration (Si2s peak) for PEGylated surface compared to the unmodified surface due to the presence of PEG groups. In contrast there was presence of F1s (684-685.5 eV) peak on the unmodified surface due to the possible contamination of the silicon wafers. The surface elemental composition of the surfaces were evaluated from the XPS survey scans using Multipak software (Table 1). The PEGylated surfaces showed an increase in the oxygen concentration due to effective C-O bonding. The silicon concentration on the PEGylated surfaces decreased due to the surface coverage with the PEG brushes. The C1s peak at 285 eV indicated higher C-C groups due to impurities on the unmodified surfaces and hence the elemental composition on the

PEGylated surfaces showed less carbon concentration. Further the thickness of the PEGylated surfaces was evaluated from the attenuation of XPS signals using the standard overlayer method<sup>77</sup>, which is given by the equation

$$I_{Si} = I_{Si}^0 \exp(-t/L_{Si}) \quad (9)$$

where  $I_{Si}^0$  is the intensity of Si2p peaks before surface modification,  $I_{Si}$  is the intensity of Si2p peaks after surface modification with PEG,  $t$  is the thickness of the film and  $L_{Si}$  is the electron attenuation for Si2p peak<sup>77</sup>. The attenuation length for Si2p at 1100 eV was found in literature to be 2.64 nm<sup>78</sup>. From the intensity of Si2p peaks before and after silanization, the thickness of the PEG silane was found to be 0.23nm.

High resolution scans were collected for carbon (C1s) using a pass energy of 10eV on the surfaces to further indicate the effective grafting of the PEG groups (Figure 16b and 16c). The high resolution C1s peaks for the PEGylated surfaces indicated two peaks, C-C peaks at 285 eV and C-O peak at 286.5 eV. The high resolution C1s peaks indicated the presence of higher characteristic C-O groups on the PEGylated surfaces due to the effective grafting of PEG groups. The unmodified surfaces indicated higher C-C peak at 285 eV and a smaller C-O peak 286.5 eV. The unmodified surface showed presence of small C-O as well as C-C peaks due to atmospheric impurities<sup>79</sup>. Further the elemental composition for the high-resolution scans were determined. The elemental composition showed as expected higher concentration of C-O bonds on the PEGylated surfaces and the unmodified surfaces showed higher concentration of C-C bonds as shown in table 2.

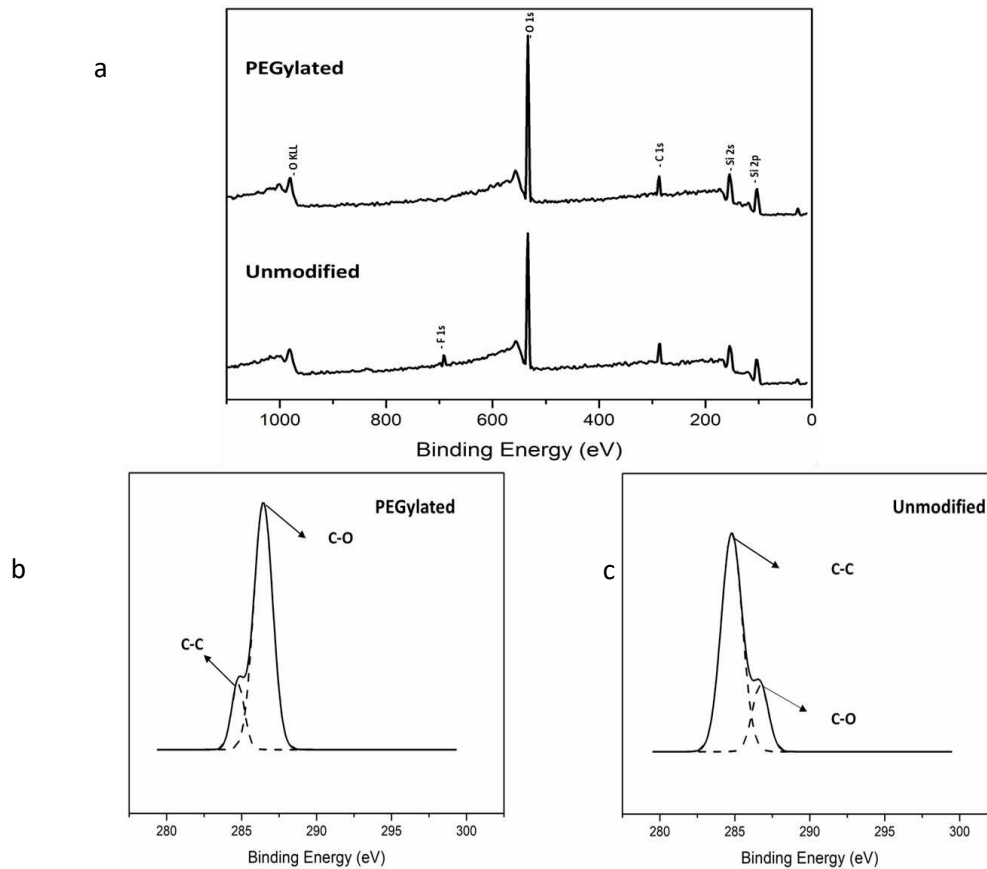


Figure 16. a) Survey scans for PEGylated and unmodified surfaces. b) High resolution scan for the PEGylated surface. c) High resolution scan for the unmodified surface

Table 1: Elemental composition of PEGylated and unmodified surfaces

Surface	% C	% O	% Si	% F
PEGylated	13.72	56.75	29.52	0
Unmodified	17.58	50.13	30.36	1.93

Table 2: Elemental composition of carbon groups on PEGylated and unmodified surfaces

Surface	% C-O	% C-C
PEGylated	84.42	15.57
Unmodified	19.18	80.811

The wettability of different surfaces was determined by measuring the static contact angles with a water droplet of volume 20  $\mu\text{L}$  using a goniometer. Hydrophilic surfaces typically display static contact angle  $\Theta < 90^\circ$ . Both PEGylated and unmodified surfaces are hydrophilic in nature. The results indicate statistically significant difference in the contact angles between PEGylated and unmodified surfaces. The static contact angles on the PEGylated surfaces were higher compared to the unmodified surfaces indicating the presence of PEG groups grafted on the surface. This was further evident from the measurement of contact angle hysteresis on the surfaces. Contact angle hysteresis is defined as the difference between the advancing and receding contact angles for a liquid droplet on a surface<sup>6</sup>. The PEGylated surfaces showed significantly lower contact angle hysteresis indicating higher chemical homogeneity due to surface coverage with the PEG brushes. The unmodified surfaces showed significantly higher contact angles hysteresis indicating lower chemical homogeneity due to the absence of PEG brushes. The high chemical homogeneity due to grafting of PEG brushes and high physical homogeneity due to low surface roughness of the PEGylated surfaces resulted in lower sliding angles for a water droplet<sup>80</sup>. The water droplet however on the unmodified surfaces had no mobility. Further the advancing contact angles of a polar and a non-polar liquid were determined to estimate the solid surface energy using the Owen Wendt relation<sup>38</sup>. The solid surface energy of the PEGylated surfaces was found to be lower than the unmodified surface. All values are indicated in table 3.

*Table 3: Table representing the wettability properties on PEGylated and unmodified surfaces*

<b>Surface</b>	<b>Contact Angle (<math>\Theta</math>)</b>	<b>Sliding Angle (<math>\alpha</math>)</b>	<b>Advancing Contact Angle (<math>\Theta_{adv}</math>)</b>	<b>Receding Contact Angle (<math>\Theta_{rec}</math>)</b>	<b>Contact Angle Hysteresis (<math>\Delta \Theta = \Theta_{adv} - \Theta_{rec}</math>)</b>	<b>Surface Energy (<math>\gamma_{sv}</math>, <math>\text{mN/m}^2</math>)</b>
Unmodified	26°	NA	34°	17°	17°	60.98
PEGylated	39°	6°	43°	37°	6°	55.29

Protein adsorption (albumin and fibrinogen) was characterized on different surfaces using a micro-BCA assay. When a surface comes into contact with blood, proteins tend to adhere to the surface after initial hydration and, hence affecting its biocompatibility<sup>72</sup>. Albumin is a water-soluble globular protein which is commonly found in blood plasma with a molecular weight of 66.5 kDa. Fibrinogen is a soluble inflammatory protein in plasma which supports thrombus generation and influences platelet adhesion/activation and aggregation. Surfaces are initially adsorbed by small proteins (Albumin) followed by larger proteins (Fibrinogen). Adsorption of proteins on different surfaces are influenced by surface characteristics like surface wettability and surface chemistry<sup>81,82</sup>. Hydrophobic surfaces have higher affinity towards protein adsorption due to hydrophobic dehydration which results in bonding of hydrophobic regions on the surface with hydrophobic domains of proteins<sup>72</sup>. Hydrophilic surfaces have lower affinity towards protein adsorption due to the strong repulsive solvation forces and energy barrier arising from the liquid adsorbed on the surface<sup>72,71</sup>. The conformational changes of the adsorbed proteins lead to inflammation, coagulation and foreign body response<sup>82</sup>. Modifying surface chemistry by activating the surfaces with reacting groups and thereby grafting specific functionality groups to the reactive groups influence the amount of proteins adsorbed<sup>82</sup>. In general, PEG groups suppress any nonspecific binding of proteins on the surfaces<sup>83</sup>. The results for albumin adsorption showed a statistically significant lower protein adsorption on the PEGylated samples when compared to the unmodified surfaces (Figure17a). Similar trend followed for fibrinogen adsorption; the results indicated statistically significant lower protein adsorption on the PEGylated samples when compared to the unmodified surfaces (Figure17b). The effective grafting of the flexible PEG brushes enhanced chemically homogeneous hydrophilicity of the surfaces thereby reducing the amount of protein adsorbed on the surface. The steric repulsive water-soluble PEG layer hence reduced protein adsorption on the surfaces<sup>84</sup>.

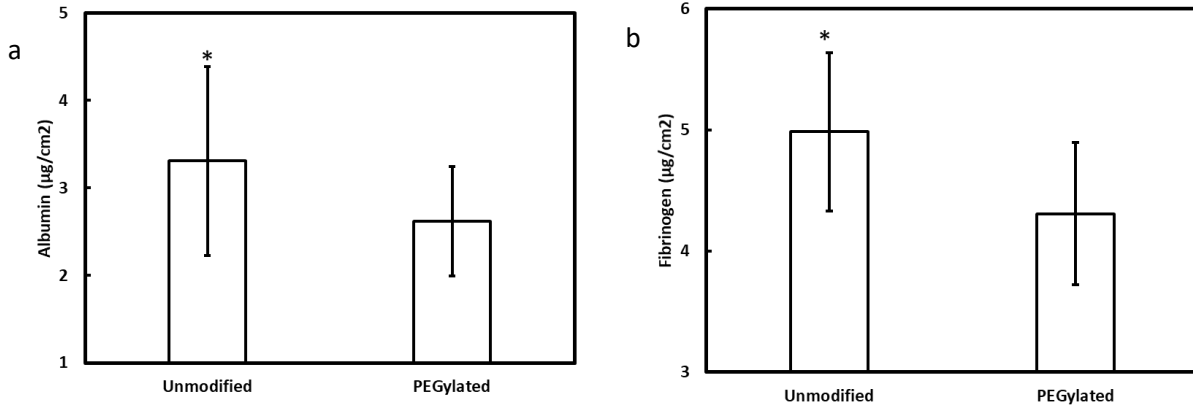


Figure 17. a) Albumin adsorption on unmodified and PEGylated surfaces. b) Fibrinogen adsorption on unmodified and PEGylated surfaces.

Cytotoxicity was evaluated on different surfaces by using Lacate dehydrogenase (LDH) assay kit. The cells in the PRP tend to die when exposed to toxic environment. As the cells die, they lose their membrane integrity and release cytoplasm and during this process, LDH enzyme is excreted. The presence of LDH enzyme indicates cytotoxicity. The results indicated the unmodified surfaces and the PEGylated surfaces had similar LDH compared to the positive control. This indicated both unmodified and the PEGylated surfaces do not induce toxicity to the cells in PRP. The LDH on the negative control was significantly higher when compared to positive control and the other surfaces (Figure 18). Hence results indicated the surfaces do not induce short term cytotoxic effects.

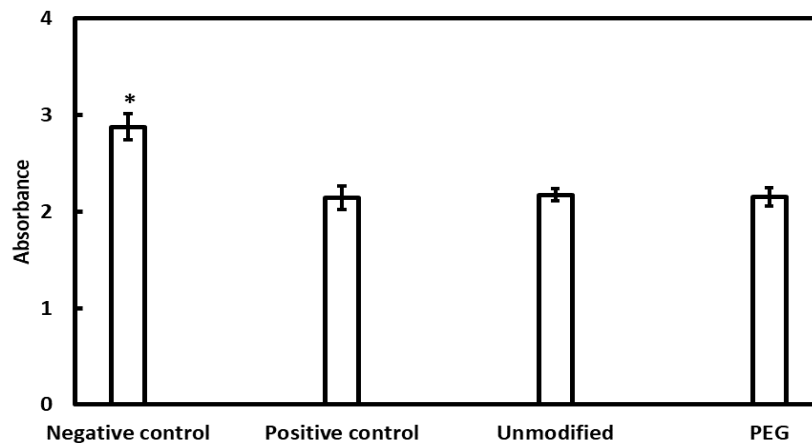
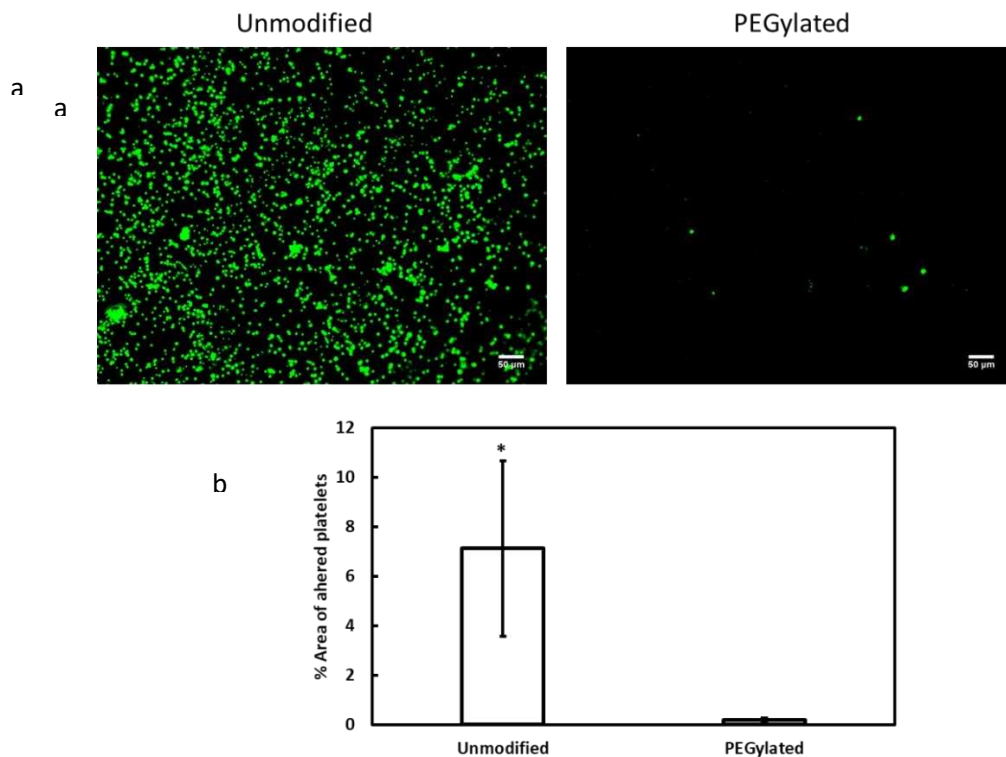


Figure 18. Absorbance values representing cell cytotoxicity of surfaces exposed to PRP.

Cell adhesion from PRP was evaluated by staining the live cells on surfaces with Calcein-AM stain and imaging them using fluorescence microscopy. Cell adhesion with bio-compatible materials play an important role in long term implantable medical devices<sup>4</sup>. Cell adhesion and activation play a critical role in formation of thrombosis which prevents regular flow of blood. PRP contains platelets and leukocytes which drive thrombosis. Hence it is important to study cell adhesion on surfaces. Cell adhesion depends on the amount of fibrinogen adhered on the surfaces, higher fibrinogen concentration on the surfaces indicate higher cell adhesion as proteins instigate cell adhesion. Fibrinogen is identified as a key protein that promotes cell adhesion at low shear stress and plays a key role in development of thrombosis<sup>4,53</sup>. Cell adhesion on the surfaces is also governed by solid-liquid interfacial area. Higher the solid-liquid interfacial area, higher is the cell adhesion on the surface<sup>9</sup>. The fluorescence microscopy images indicate higher cell adhesion on the unmodified surfaces compared to the PEGylated surfaces (Figure19a). The protein adsorbed on the PEGylated samples were significantly less as concluded from the protein adsorption test and hence the cell adhesion is low compared to unmodified surfaces. The cell adhesion was further estimated by measuring the percentage area of live cells (green color) adhered on the surfaces using ImageJ software. The analysis indicated statistically significant difference between PEGylated and unmodified surfaces. The percentage area of the live cells adhered on the unmodified surfaces were statistically significantly higher than the PEGylated surfaces (Figure19b). The PEGylated surfaces have lower solid-blood interfacial area due to the presence of water-soluble PEG layer and hence display significantly lower cell adhesion. The higher cell adhesion on the unmodified surfaces is due to higher solid-blood interfacial area.



*Figure 19. a) Fluorescence microscopy images indicating cell (Live) adhesion from PRP on unmodified and PEGylated surfaces. b) Percentage area of cells adhered on unmodified and PEGylated surfaces using ImageJ.*

The platelets and leukocytes adhered on different surfaces were identified by staining the adhered cells using DAPI (4, 6 – diamidino – 2 – phenylindole) and Rhodamine Phalloidin and imaging them using fluorescence microscope. DAPI is a blue fluorescent dye which is used to detect leukocytes whereas rhodamine phalloidin stains both platelets and leukocytes red. Platelets adhered to the surface tend to become activated and aggregated which lead to thrombus formation there by reducing the surrounding platelet count<sup>4</sup>. The adhered platelets tend to promote leukocyte adhesion<sup>85</sup>. Adhesion between platelets and leukocytes lead to the formation of aggregates which increases platelet activation rate<sup>86</sup>. The adhered leukocytes tend to release platelet activation factor which enhance local platelet activation<sup>86,87</sup>. Hence it is important to study platelet-leukocyte interactions on the surfaces. The fluorescence microscopy images indicate significantly higher platelets and leukocytes on the unmodified surfaces compared to the

PEGylated surfaces. DAPI results indicated significant increase in the leukocytes (blue color) adhesion on the unmodified surfaces (Figure 20a). Similar trend followed for Rhodamine-Phalloidin (red color) which also indicated significant increase in platelet and leukocytes adhesion on the unmodified surfaces (Figure 20a). The cell identification was further estimated by measuring the percentage area of platelets and leukocytes adhered on the surfaces using ImageJ software. The analysis indicated statistically significant difference between PEGylated and unmodified surfaces. The percentage area of the platelets and leukocytes adhered on the unmodified surfaces were statistically significantly higher than the PEGylated surfaces (Figure 20b). The results followed similar trend as that of cell adhesion studies.

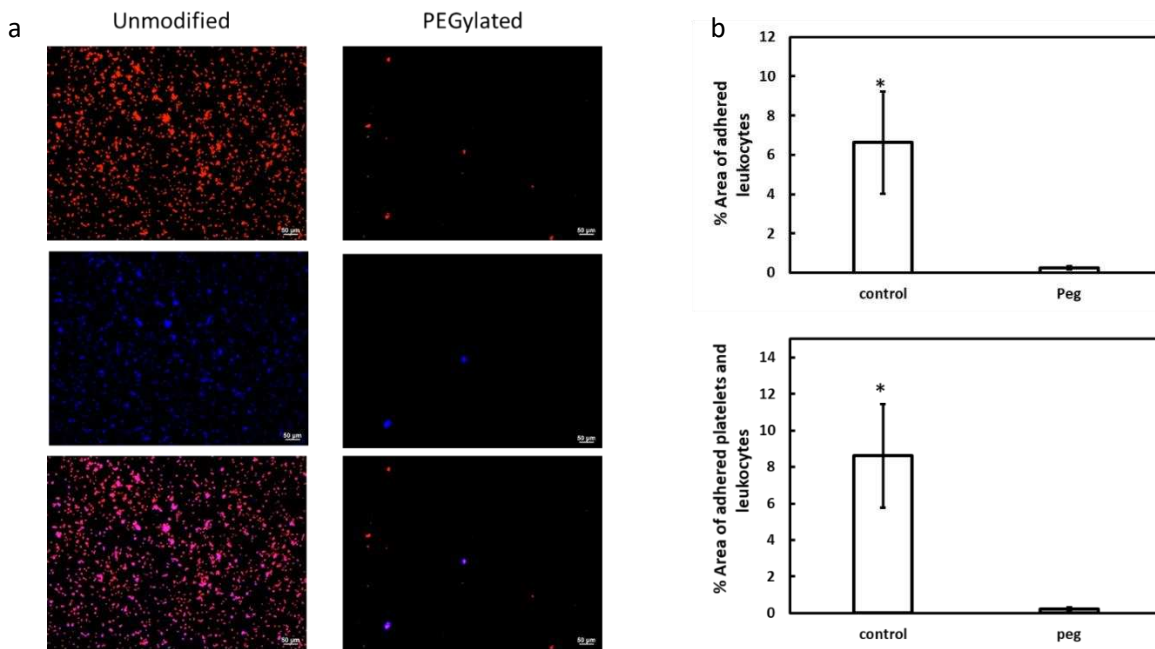
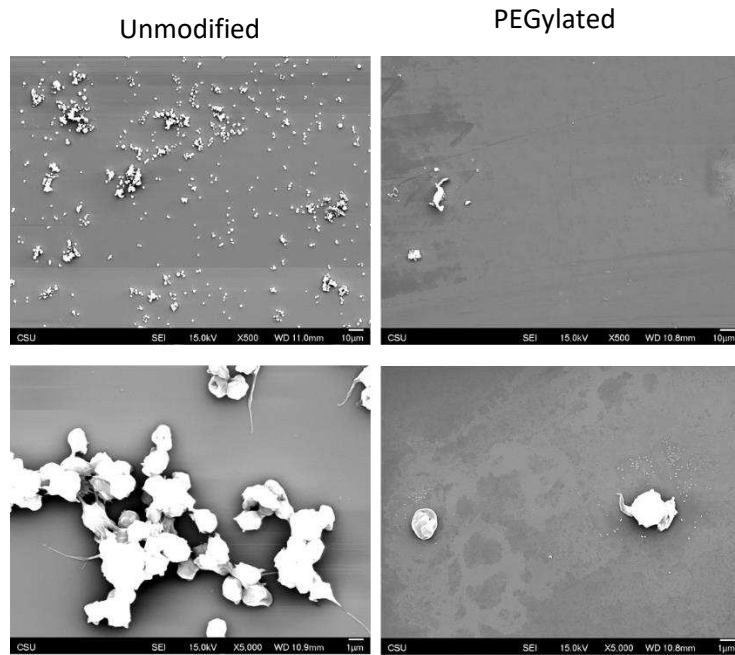


Figure 20. a) Fluorescence microscopy images indicating platelets and leukocytes adhesion using DAPI and Rhodamine-Phalloidin stain on unmodified and PEGylated surfaces. b) Percentage area of adhered platelets and leukocytes on unmodified and PEGylated surfaces using ImageJ.

Platelet activation was evaluated on different surfaces using SEM. Platelets adhered on the surfaces tend to get activated and mediate platelet aggregation and thrombus formation<sup>53,88</sup>. The adhered platelets change their shape to increase the adhesion area of the platelets and

activate other platelets surrounding them<sup>88</sup>. Hence it is important to evaluate platelet activation and aggregation on the surfaces. SEM images (Figure 20) at 500X indicated higher platelet adhesion on the unmodified surfaces as compared to the PEGylated surfaces. Further the SEM images (Figure 21) at 5000X indicated changes in the platelet morphology on the unmodified surfaces. The platelets on the unmodified surfaces tend to exhibit dendritic behavior indicating platelet activation. The unmodified surfaces also indicated platelet-platelet contact resulting in platelet aggregation. Such behavior was not seen on the PEGylated surfaces due to low platelet adhesion on the surfaces.



*Figure 21. Scanning electron microscope images of leukocytes and platelets adhesion on unmodified and PEGylated surfaces.*

Blood clot is formed through coagulation which involves platelet adhesion, activation and aggregation as well as formation of fibrin mesh<sup>54</sup>. The fibrin mesh tends to trap RBC's constituted by hemoglobin. During the blood clot, the RBC's are trapped inside the fibrin mesh and when the surfaces are rinsed with DI water, the RBC's that are free in blood get lysed releasing hemoglobin due to the change in pressure when exposed to water<sup>69,88,89</sup>. The amount of free hemoglobin on

the surfaces after exposure to whole blood was evaluated using a plate reader. Lower amount of hemoglobin indicates more blood clotting on the surface. After specific intervals of time, 2mL of DI water was added on each surface to measure the amount of free hemoglobin. The results indicated significant delayed blood clotting on the PEGylated surfaces when compared to the unmodified surfaces (Figure 22). The amount of free hemoglobin decreased drastically on the unmodified surfaces from 15 mins to 30 mins. The amount of free hemoglobin on the PEGylated surfaces however did not show a drastic change over the course of 45 mins. The whole blood clotting results were in accordance with the protein adsorption, as lower protein adsorption indicates delayed blood clotting on the surfaces.

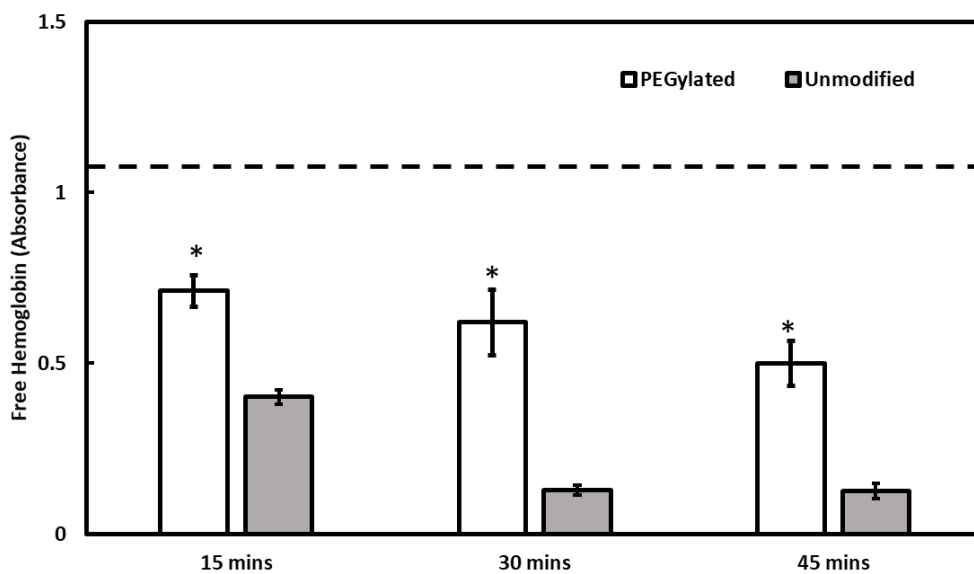
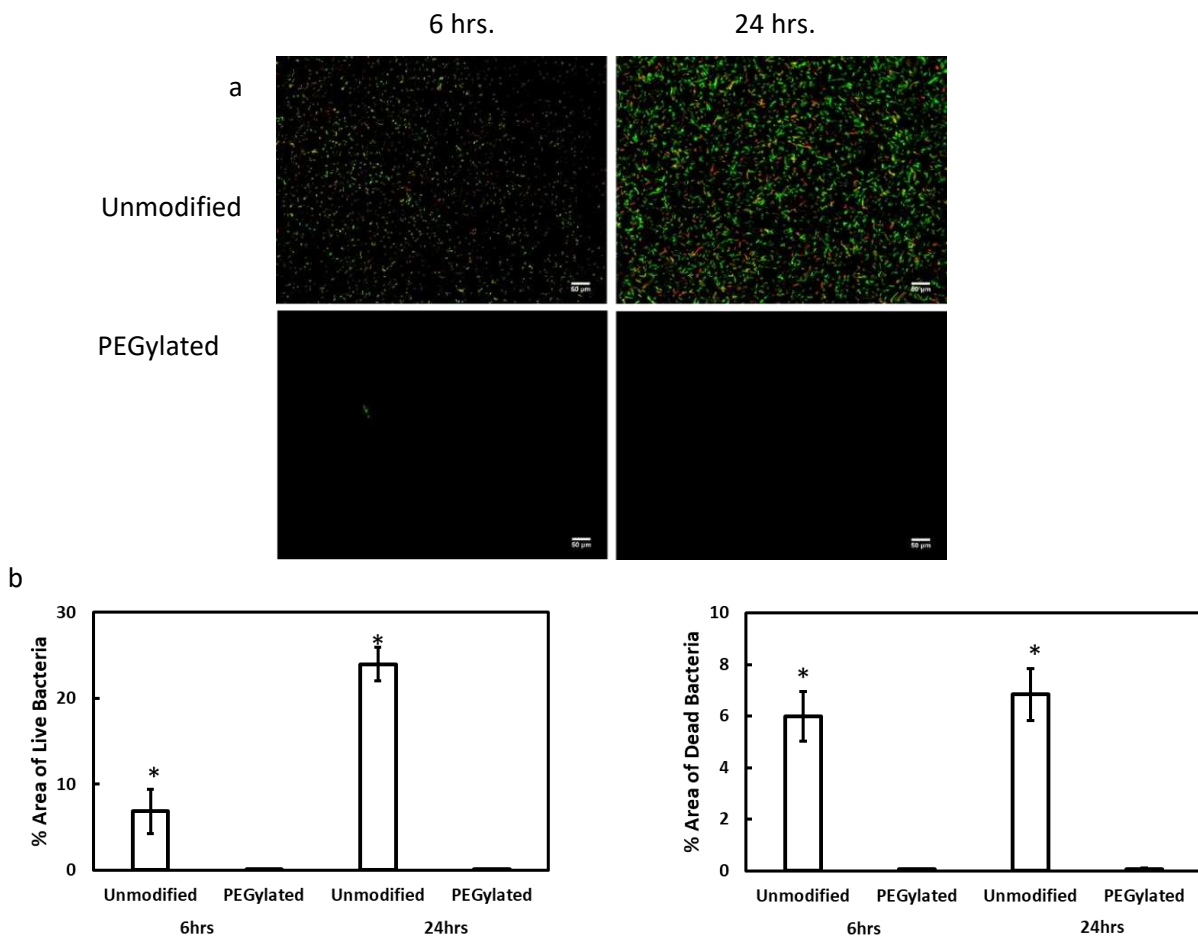


Figure 22. Whole human blood clotting on unmodified and PEGylated surfaces after 15, 30 and 45mins (dashed line indicates the amount of free haemoglobin in un-clotted blood).

Bacterial adhesion on surfaces lead to the formation of biofilms which enhance the growth of bacteria colonies<sup>56</sup>. Bacterial adhesion is a serious issue especially with blood contacting medical devices<sup>58</sup>. The reduction of bacterial infections on surfaces is crucial to reduce medical device failures. Bacteria groups are commonly divided into gram-positive and gram-

negative bacteria<sup>90,91</sup>. Gram-positive bacteria have cell wall thickness of 20-80nm thickness, have low lipid content and high peptidoglycan content<sup>90,91</sup>. Gram-negative bacteria have cell wall thickness of 8-12 nm thickness, have high lipid content and low peptidoglycan content<sup>90,91</sup>. Staphylococcus Aureus is a gram positive bacteria and Escherichia Coli is a gram negative bacteria which has been used in this bacterial adhesion study<sup>90,91</sup>. Bacterial adhesion was evaluated using fluorescence microscope and SEM. The stain propidium iodide stains the dead bacteria by staining the dead cells (Red color) while the SYTO™ 9 stains the live bacteria (Green color) on the surfaces. The fluorescence microscopy results for E Coli indicated significantly higher adhesion of bacteria on the unmodified surfaces for both 6 hrs and 24 hrs of bacterial incubation (Figure 23a). The PEGylated surfaces on the other hand showed significantly lower bacterial adhesion for 6 hrs and 24 hrs of bacterial incubation (Figure 23a). The bacterial adhesion on the surfaces incubated for 24 hrs indicated significantly higher Live and Dead bacterial adhesion than 6 hrs of incubation on the unmodified surfaces (Figure 23a). This was expected due to increase in incubation time which would lead to increase in bacterial adhesion on the surfaces.



*Figure 23a) Fluorescence microscopy images indicating bacterial adhesion (E. Coli) on the surfaces after 6 hrs and 24 hrs of incubation. b) Percentage area of Live and Dead E Coli adhered on the surfaces.*

Similar trends followed for S Aureus as the results indicated significantly higher adhesion of bacteria on the unmodified surfaces for both 6 hrs and 24 hrs of bacterial incubation (Figure 24a). The PEGylated surfaces on the other hand showed significantly lower bacterial adhesion for 6 hrs and 24 hrs of bacterial incubation (Figure 24a). The bacterial adhesion on the surfaces incubated for 24 hrs indicated significantly higher Live and Dead bacterial adhesion than 6 hrs of incubation on the unmodified surfaces (Figure 24a). The effective grafting of PEG brushes led to the reduce in the surface energy along with reduced protein adsorption which led to reduced bacterial adhesion on the PEGylated surfaces. The bacterial adhesion was further estimated by measuring the percentage area of Live/Dead bacteria adhered on the surfaces using ImageJ

software. The analysis indicated statistically significant difference between PEGylated and unmodified surfaces. The percentage area of the Live and Dead bacteria for E Coli (Figure 23b) and S Aureus (Figure 24b) adhered on the unmodified surfaces were statistically significantly higher than the PEGylated surfaces at 6hrs and 24 hrs of incubation.

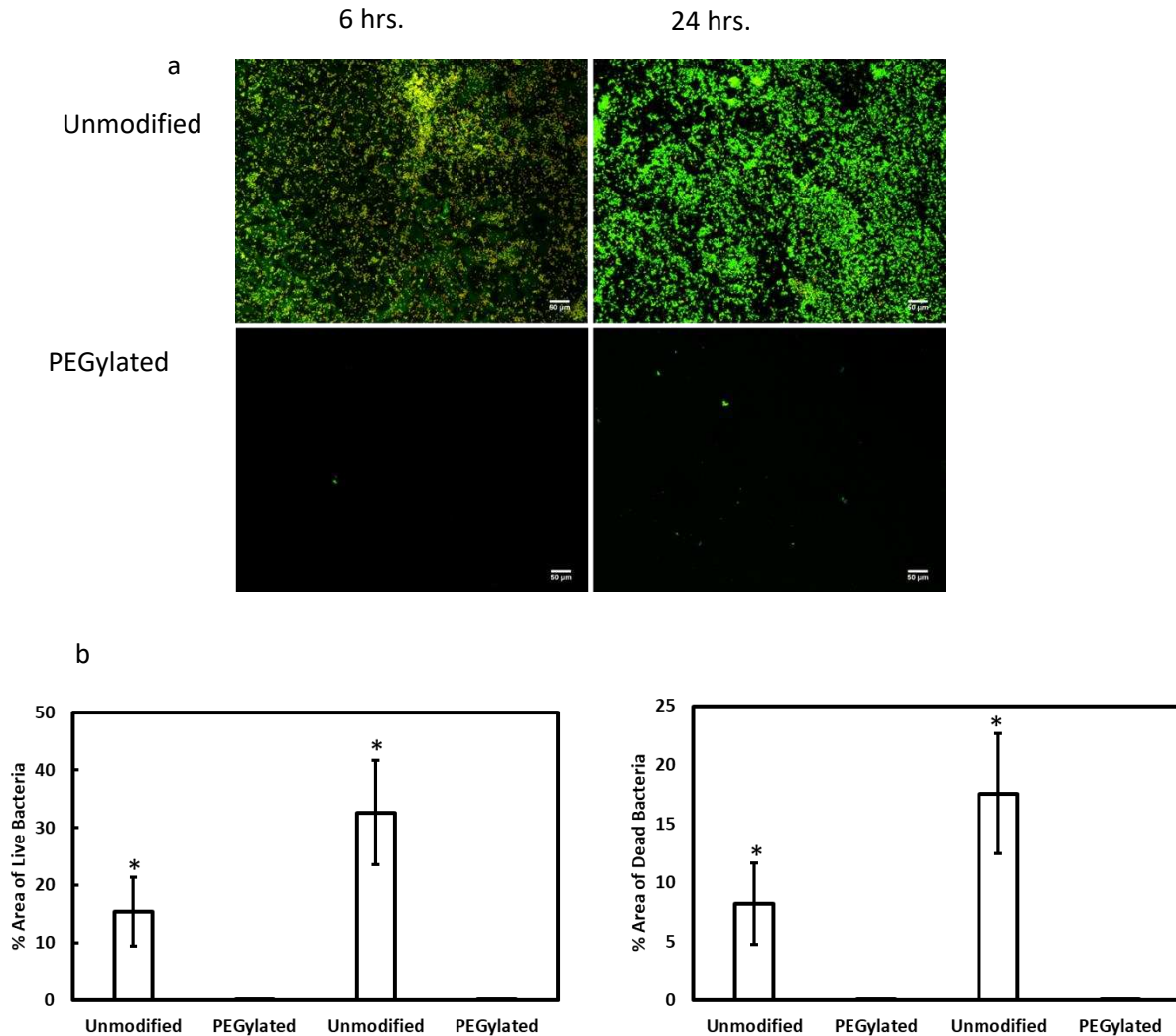


Figure 24. a) Fluorescence microscopy images indicating bacterial adhesion (*S. Aureus*) on the surfaces after 6 hrs and 24 hrs of incubation. b) Percentage area of Live and Dead *S. Aureus* adhered on the surfaces.

SEM was used to evaluate the morphology of the bacteria adhered on the surfaces. The SEM images showed consistent results as with the fluorescence microscopy. The unmodified surfaces indicated higher bacterial adhesion for E Coli (Figure25) and S Aureus (Figure26) at

6hrs and 24 hrs of incubation. The bacterial adhesion was higher at 24 hrs of incubation on the unmodified surfaces when compared to 6 hrs of incubation for both groups of bacteria. The SEM images also showed a significant decrease in bacterial adhesion on the PEGylated samples for 6 hrs and 24 hrs of incubation when compared to unmodified surfaces. The reduced surface energy of the PEGylated surfaces with their tendency to reduce protein adsorption on the surfaces led to the reduction in bacteria adhered on the surfaces.

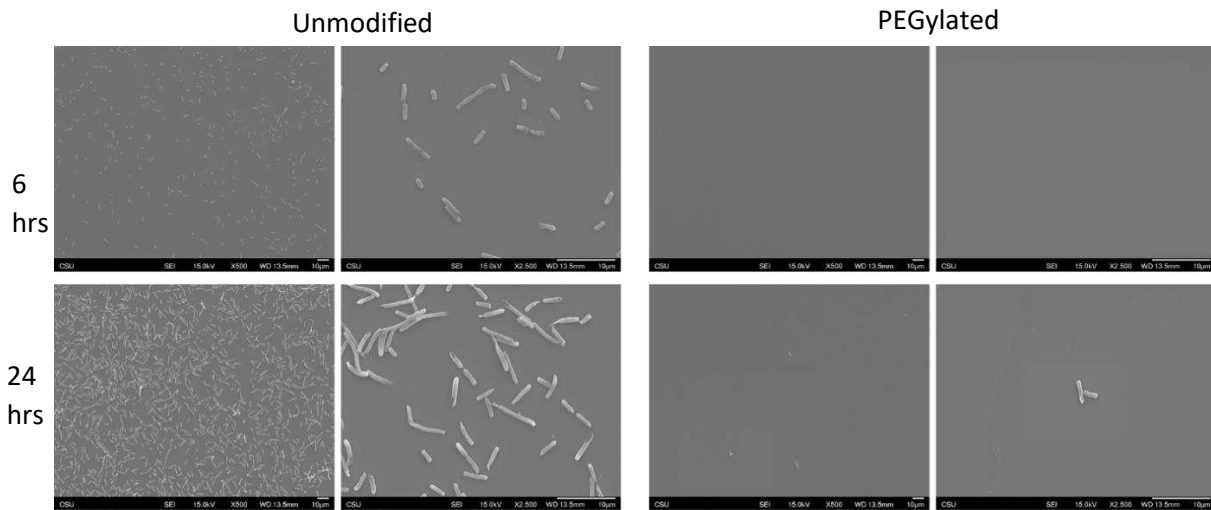


Figure 25. Scanning electron microscopy images indicating bacterial adhesion (*E. Coli*) on the surfaces after 6 hrs and 24 hrs of incubation.

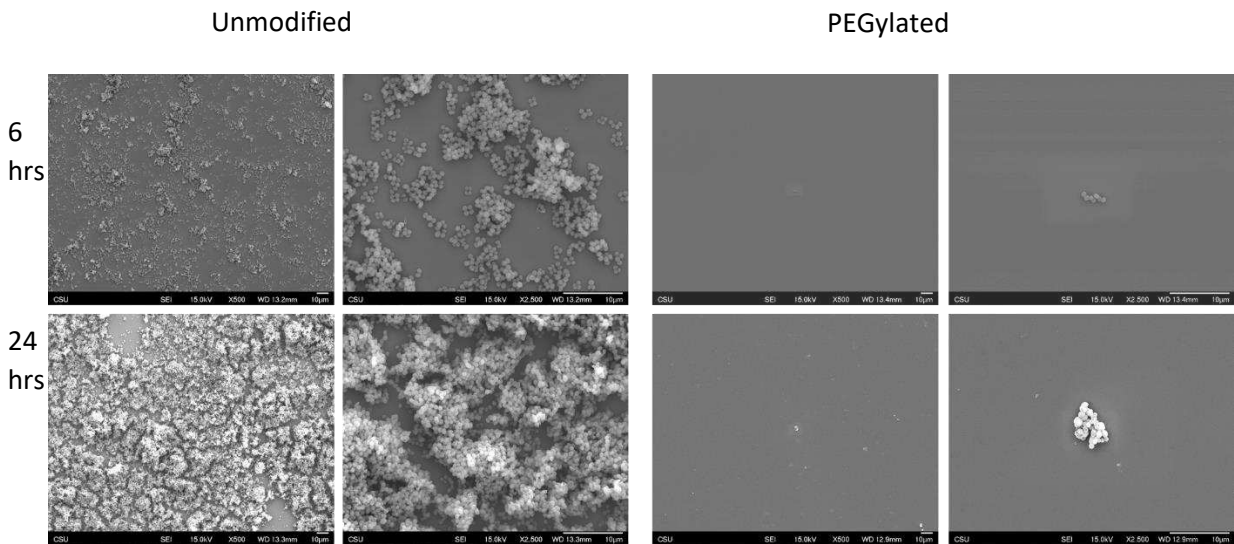


Figure 26. Scanning electron microscopy images indicating bacterial adhesion (*S. Aureus*) on the surfaces after 6 hrs and 24 hrs of incubation.

## CHAPTER 4

### Conclusions and Future Work

#### 4.1 Conclusions

We successfully designed dual superlyophobic surfaces by combining re-entrant texture and appropriate surface energy with the recently discovered recyclable polymer. We fabricated these surfaces using a simple spray coating method that resulted in textured surfaces with re-entrant textures. The surface energy of these surfaces was then modified by plasma treatment which then displayed dual superlyophobic properties which was characterized both underwater and under-oil. Further, these surfaces were successfully utilised for underwater manipulation of ferrofluid droplets in which both the movement and splitting of the droplets were shown. We further spray coated the polymer on thin aluminium meshes in order to show effective oil-water separation where the oil-water mixtures were successfully separated on pre-wetted surfaces with an efficiency of 99%.

We also successfully developed polyethylene glycol based hydrophilic slippery surfaces by covalently attaching PEG silane via O-Si bonds to hydroxylated surface to form PEG brushes. The hydrophilic slippery surfaces formed were chemically homogeneous with low molecular weight PEG brushes with high grafting density. These surfaces can easily repel high surface tension liquids like water and blood with a tilt angle of  $6^\circ$ . The PEGylated surfaces successfully reduced protein adsorption on the surface along with reduction in cell and bacterial adhesion on the surfaces. The results also indicated delayed blood clotting on the PEGylated surfaces when compared to the unmodified surfaces.

#### 4.2 Future Work

Dual superlyophobic surfaces displayed both underwater superoleophobicity and under-oil superhydrophobicity. We demonstrated potential underwater manipulation of oil based

ferrofluid using an external magnet. We would like to also study underoil manipulation of water based ferrofluid in the future. We also demonstrated oil-water separations but we would extend this to analyze the separation of micro/nano emulsions on these surfaces.

PEGylated hydrophilic surfaces were successfully developed to delay blood clotting, reduce protein adsorption, cell and bacterial adhesion. We would like to test these surfaces under dynamic conditions which would replicate similar flow conditions inside the body. We would like to see if it is possible to polish titanium and its alloys as smooth as silicon and impart the concept of slipperiness since titanium are widely used as implants. We would like to conduct tests with tyrode both under static and dynamic conditions to check the stability of these PEGylated surfaces over time.

## References

1. Xue, C. H. *et al.* Self-roughened superhydrophobic coatings for continuous oil-water separation. *J. Mater. Chem. A* **3**, 10248–10253 (2015).
2. Wang, X., Yu, J., Sun, G. & Ding, B. Electrospun nanofibrous materials: a versatile medium for effective oil/water separation. *Materials Today* vol. 19 403–414 (2016).
3. Xiong, Z. *et al.* Robust superhydrophilic polylactide (PLA) membranes with a TiO<sub>2</sub> nanoparticle inlaid surface for oil/water separation. *J. Mater. Chem. A* **5**, 6538–6545 (2017).
4. Jaffer, I. H., Fredenburgh, J. C., Hirsh, J. & Weitz, J. I. Medical device-induced thrombosis: What causes it and how can we prevent it? *Journal of Thrombosis and Haemostasis* vol. 13 S72–S81 (2015).
5. Hamzeh-Cognasse, H. *et al.* Platelets and infections - Complex interactions with bacteria. *Frontiers in Immunology* vol. 6 82 (2015).
6. Kota, A. K., Kwon, G. & Tuteja, A. The design and applications of superomniphobic surfaces. *NPG Asia Materials* vol. 6 e109–e109 (2014).
7. Wang, W. *et al.* Superhydrophobic Coatings with Edible Materials. *ACS Appl. Mater. Interfaces* **8**, 18664–18668 (2016).
8. Beemer, D. L., Wang, W. & Kota, A. K. Durable gels with ultra-low adhesion to ice. *J. Mater. Chem. A* **4**, 18253–18258 (2016).
9. Movafaghi, S. *et al.* Hemocompatibility of super-repellent surfaces: Current and future. *Materials Horizons* vol. 6 1596–1610 (2019).
10. Movafaghi, S. *et al.* Tunable superomniphobic surfaces for sorting droplets by surface tension. *Lab Chip* **16**, 3204–3209 (2016).
11. Wang, W. *et al.* Metamorphic Superomniphobic Surfaces. *Adv. Mater.* **29**, 1700295

- (2017).
12. Butt, H.-J. *et al.* *Characterization of super liquid-repellent surfaces.* *Ciro Semprebon Current Opinion in Colloid & Interf. Sci* vol. 19 (2014).
  13. Contact angle hysteresis: a review of fundamentals and applications Publisher Springer-Verlag. doi:10.1007/s00396-012-2796-6.
  14. Thomas Young, B. & For Sec, M. D. *HI, An Essay on the Cohesion of Fluids.*
  15. Kota, A. K., Choi, W. & Tuteja, A. Superomniphobic surfaces: Design and durability. *MRS Bull.* **38**, 383–390 (2013).
  16. Wang, Y., Orol, D., Owens, J., Simpson, K. & Lee, H. J. Design and Development of Anti-Icing Aluminum Surface. *Mater. Sci. Appl.* **4**, 347–356 (2013).
  17. Wenzel, R. N. Resistance of solid surfaces to wetting by water. *Ind. Eng. Chem.* **28**, 988–994 (1936).
  18. Cassie, A. B. D. Contact angles. *Discussions of the Faraday Society* vol. 3 11–16 (1948).
  19. Vahabi, H. *et al.* Metallic superhydrophobic surfaces via thermal sensitization. *Appl. Phys. Lett.* **110**, 251602 (2017).
  20. Bartlet, K., Movafaghi, S., Dasi, L. P., Kota, A. K. & Popat, K. C. Antibacterial activity on superhydrophobic titania nanotube arrays. *Colloids Surfaces B Biointerfaces* **166**, 179–186 (2018).
  21. Vallabhuneni, S., Movafaghi, S., Wang, W. & Kota, A. K. Superhydrophobic Coatings for Improved Performance of Electrical Insulators. *Macromol. Mater. Eng.* **303**, 1800313 (2018).
  22. Yong, J., Chen, F., Yang, Q., Huo, J. & Hou, X. Superoleophobic surfaces. *Chemical Society Reviews* vol. 46 4168–4217 (2017).

23. Kota, A. K., Kwon, G. & Tuteja, A. The design and applications of superomniphobic surfaces. *NPG Asia Mater.* **6**, 109 (2014).
24. Bonn, D., Eggers, J., Indekeu, J. & Meunier, J. Wetting and spreading. *Rev. Mod. Phys.* **81**, 739–805 (2009).
25. Cao, G. *et al.* Dually Prewetted Underwater Superoleophobic and under Oil Superhydrophobic Fabric for Successive Separation of Light Oil/Water/Heavy Oil Three-Phase Mixtures. *ACS Appl. Mater. Interfaces* **9**, 36368–36376 (2017).
26. Zhou, W. *et al.* Dual Superlyophobic Copper Foam with Good Durability and Recyclability for High Flux, High Efficiency, and Continuous Oil-Water Separation. *ACS Appl. Mater. Interfaces* **10**, 9841–9848 (2018).
27. Cheng, L. *et al.* Fouling-Resistant and Self-Cleaning Aliphatic Polyketone Membrane for Sustainable Oil-Water Emulsion Separation. *ACS Appl. Mater. Interfaces* **10**, 44880–44889 (2018).
28. Chen, K., Zhou, S. & Wu, L. Self-healing underwater superoleophobic and antibiofouling coatings based on the assembly of hierarchical microgel spheres. *ACS Nano* **10**, 1386–1394 (2016).
29. Kota, A. K., Kwon, G., Choi, W., Mabry, J. M. & Tuteja, A. Hygro-responsive membranes for effective oil-water separation. *Nat. Commun.* **3**, 1–8 (2012).
30. Xu, J. *et al.* Droplet-based microfluidic device for multiple-droplet clustering. *Lab Chip* **12**, 725–730 (2012).
31. Shembekar, N., Chaipan, C., Utharala, R. & Merten, C. A. Droplet-based microfluidics in drug discovery, transcriptomics and high-throughput molecular genetics. *Lab on a Chip* vol. 16 1314–1331 (2016).
32. Tian, X., Jokinen, V., Li, J., Sainio, J. & Ras, R. H. A. Unusual Dual Superlyophobic

- Surfaces in Oil–Water Systems: The Design Principles. *Adv. Mater.* **28**, 10652–10658 (2016).
33. Yong, J., Yang, Q., Guo, C., Chen, F. & Hou, X. A review of femtosecond laser-structured superhydrophobic or underwater superoleophobic porous surfaces/materials for efficient oil/water separation. *RSC Advances* vol. 9 12470–12495 (2019).
  34. Li, Z. & Guo, Z. Bioinspired surfaces with wettability for antifouling application. *Nanoscale* vol. 11 22636–22663 (2019).
  35. Li, J. *et al.* Underoil superhydrophilic desert sand layer for efficient gravity-directed water-in-oil emulsions separation with high flux. *J. Mater. Chem. A* **6**, 223–230 (2017).
  36. Yihan, S., Mingming, L. & Guo, Z. Ag nanoparticles loading of polypyrrole-coated superwetting mesh for on-demand separation of oil-water mixtures and catalytic reduction of aromatic dyes. *J. Colloid Interface Sci.* **527**, 187–194 (2018).
  37. Zhao, P., Qin, N., Ren, C. L. & Wen, J. Z. Polyamide 6.6 separates oil/water due to its dual underwater oleophobicity/underoil hydrophobicity: Role of 2D and 3D porous structures. *Appl. Surf. Sci.* **466**, 282–288 (2019).
  38. Owens, D. K. & Wendt, R. C. Estimation of the surface free energy of polymers. *J. Appl. Polym. Sci.* **13**, 1741–1747 (1969).
  39. Zhang, X., Sun, L., Yu, Y. & Zhao, Y. Flexible Ferrofluids: Design and Applications. *Advanced Materials* vol. 31 1903497 (2019).
  40. Zhu, P. & Wang, L. Passive and active droplet generation with microfluidics: a review. *Lab Chip* **17**, 34–75 (2017).
  41. Latikka, M., Backholm, M., Timonen, J. V. I. & Ras, R. H. A. Wetting of ferrofluids: Phenomena and control. *Current Opinion in Colloid and Interface Science* vol. 36 118–129 (2018).

42. Teh, S. Y., Lin, R., Hung, L. H. & Lee, A. P. Droplet microfluidics. *Lab on a Chip* vol. 8 198–220 (2008).
43. Zhang, K. *et al.* On-demand microfluidic droplet manipulation using hydrophobic ferrofluid as a continuous-phase. *Lab Chip* **11**, 1271–1275 (2011).
44. Banerjee, U. & Sen, A. K. Shape evolution and splitting of ferrofluid droplets on a hydrophobic surface in the presence of a magnetic field. *Soft Matter* **14**, 2915–2922 (2018).
45. Huang, G. *et al.* Magnetically actuated droplet manipulation and its potential biomedical applications. *ACS Applied Materials and Interfaces* vol. 9 1155–1166 (2017).
46. Wang, B., Liang, W., Guo, Z. & Liu, W. Biomimetic super-lyophobic and super-lyophilic materials applied for oil/water separation: A new strategy beyond nature. *Chemical Society Reviews* vol. 44 336–361 (2015).
47. Cao, C. & Cheng, J. A novel Cu(OH)<sub>2</sub> coated filter paper with superhydrophobicity for the efficient separation of water-in-oil emulsions. *Mater. Lett.* **217**, 5–8 (2018).
48. Crick, C. R., Ozkan, F. T. & Parkin, I. P. Fabrication of optimized oil–water separation devices through the targeted treatment of silica meshes.  
<http://www.tandfonline.com/action/journalInformation?show=aimsScope&journalCode=tst a20#.VmBmuzZFCUk> (2015) doi:10.1088/1468-6996/16/5/055006.
49. Xu, C. L. & Wang, Y. Z. Novel dual superlyophobic materials in water-oil systems: Under oil magneto-fluid transportation and oil-water separation. *J. Mater. Chem. A* **6**, 2935–2941 (2018).
50. Popat, K. C., Eltgroth, M., LaTempa, T. J., Grimes, C. A. & Desai, T. A. Titania nanotubes: A novel platform for drug-eluting coatings for medical implants? *Small* **3**, 1878–1881 (2007).

51. Milner, K. R., Snyder, A. J. & Siedlecki, C. A. Sub-micron texturing for reducing platelet adhesion to polyurethane biomaterials. *J. Biomed. Mater. Res. - Part A* **76**, 561–570 (2006).
52. Xu, L. C. & Siedlecki, C. A. Protein adsorption, platelet adhesion, and bacterial adhesion to polyethylene-glycol-textured polyurethane biomaterial surfaces. *J. Biomed. Mater. Res. - Part B Appl. Biomater.* **105**, 668–678 (2017).
53. Gorbet, M. B. & Sefton, M. V. Biomaterial-associated thrombosis: Roles of coagulation factors, complement, platelets and leukocytes. *Biomaterials* vol. 25 5681–5703 (2004).
54. Wilson, A. C., Neuenschwander, P. F. & Chou, S.-F. Engineering Approaches to Prevent Blood Clotting from Medical Implants. doi:10.33552/ABEB.2018.01.000510.
55. Muscente, F. & De Caterina, R. Risk of stroke after transcatheter aortic valve implant: the role of the new oral anticoagulants. doi:10.1093/eurheartj/suz016.
56. Sandoe, J. A. T., Witherden, I. R., Cove, J. H., Heritage, J. & Wilcox, M. H. Correlation between enterococcal biofilm formation in vitro and medical-device-related infection potential in vivo. *J. Med. Microbiol.* **52**, 547–550 (2003).
57. Khatoon, Z., McTiernan, C. D., Suuronen, E. J., Mah, T. F. & Alarcon, E. I. Bacterial biofilm formation on implantable devices and approaches to its treatment and prevention. *Heliyon* vol. 4 e01067 (2018).
58. Darouiche, R. O. Device-Associated Infections: A Macroproblem that Starts with Microadherence. *Clin. Infect. Dis.* **33**, 1567–1572 (2001).
59. Chouirfa, H., Bouloussa, H., Migonney, V. & Falentin-Daudré, C. Review of titanium surface modification techniques and coatings for antibacterial applications. *Acta Biomaterialia* vol. 83 37–54 (2019).
60. Sidambe, A. Biocompatibility of Advanced Manufactured Titanium Implants—A Review.

- Materials (Basel)*. **7**, 8168–8188 (2014).
61. Abdel-Hady Gepreel, M. & Niinomi, M. Biocompatibility of Ti-alloys for long-term implantation. *Journal of the Mechanical Behavior of Biomedical Materials* vol. 20 407–415 (2013).
  62. Huang, N. *et al.* Hemocompatibility of titanium oxide films. *Biomaterials* **24**, 2177–2187 (2003).
  63. Walkowiak-Przybyło, M. *et al.* Adhesion, activation, and aggregation of blood platelets and biofilm formation on the surfaces of titanium alloys Ti6Al4V and Ti6Al7Nb. *J. Biomed. Mater. Res. - Part A* **100 A**, 768–775 (2012).
  64. Moradi, S., Hadjesfandiari, N., Toosi, S. F., Kizhakkedathu, J. N. & Hatzikiriakos, S. G. Effect of Extreme Wettability on Platelet Adhesion on Metallic Implants: From Superhydrophilicity to Superhydrophobicity. *ACS Appl. Mater. Interfaces* **8**, 17631–17641 (2016).
  65. Kasemo, B. & Gold, J. Implant surfaces and interface processes. *Adv. Dent. Res.* **13**, 8–20 (1999).
  66. Narain, R., Wang, Y., Ahmed, M., Lai, B. F. L. & Kizhakkedathu, J. N. Blood components interactions to ionic and nonionic glyconanogels. *Biomacromolecules* **16**, 2990–2997 (2015).
  67. Popat, K. C., Mor, G., Grimes, C. A. & Desai, T. A. Surface modification of nanoporous alumina surfaces with poly(ethylene glycol). *Langmuir* **20**, 8035–8041 (2004).
  68. Jokinen, V., Kankuri, E., Hoshian, S., Franssila, S. & Ras, R. H. A. Blood-Repellent Surfaces: Superhydrophobic Blood-Repellent Surfaces (Adv. Mater. 24/2018). *Adv. Mater.* **30**, 1870173 (2018).
  69. Sabino, R. M., Kauk, K., Movafaghi, S., Kota, A. & Popat, K. C. Interaction of blood

- plasma proteins with superhemophobic titania nanotube surfaces. *Nanomedicine Nanotechnology, Biol. Med.* **21**, 102046 (2019).
70. Khorasani, M. T. & Mirzadeh, H. In vitro blood compatibility of modified PDMS surfaces as superhydrophobic and superhydrophilic materials. *J. Appl. Polym. Sci.* **91**, 2042–2047 (2004).
  71. Vogler, E. A. Protein adsorption in three dimensions. *Biomaterials* **33**, 1201–1237 (2012).
  72. Aiyelabegan, H. T. & Sadroddiny, E. Fundamentals of protein and cell interactions in biomaterials. *Biomedicine and Pharmacotherapy* vol. 88 956–970 (2017).
  73. Kovach, K. M., Capadona, J. R., Gupta, A. Sen & Potkay, J. A. The effects of PEG-based surface modification of PDMS microchannels on long-term hemocompatibility. *J. Biomed. Mater. Res. - Part A* **102**, 4195–4205 (2014).
  74. Pacharra, S. *et al.* Surface patterning of a novel PEG-functionalized poly-L-lactide polymer to improve its biocompatibility: Applications to bioresorbable vascular stents. *J. Biomed. Mater. Res. - Part B Appl. Biomater.* **107**, 624–634 (2019).
  75. Su, X., Hao, D., Li, Z., Guo, X. & Jiang, L. Design of hierarchical comb hydrophilic polymer brush (HCHPB) surfaces inspired by fish mucus for anti-biofouling. *J. Mater. Chem. B* **7**, 1322–1332 (2019).
  76. Liu, X. *et al.* Blood compatible materials: state of the art. **2**, 5709–5926.
  77. Petrovykh, D. Y., Kimura-Suda, H., Tarlov, M. J. & Whitman, L. J. Quantitative Characterization of DNA Films by X-ray Photoelectron Spectroscopy. *Langmuir* **20**, 429–440 (2004).
  78. Powell, C. J. & Jablonski, A. Electron effective attenuation lengths for applications in Auger electron spectroscopy and x-ray photoelectron spectroscopy. *Surf. Interface Anal.* **33**, 211–229 (2002).

79. Sharma, S., Johnson, R. W. & Desai, T. A. XPS and AFM analysis of antifouling PEG interfaces for microfabricated silicon biosensors. *Biosens. Bioelectron.* **20**, 227–239 (2004).
80. HYDROPHILIC, YET SLIPPERY SOLID SURFACES.  
<http://www.freepatentsonline.com/20190152201.pdf>.
81. Xu, L. C. & Siedlecki, C. A. Effects of surface wettability and contact time on protein adhesion to biomaterial surfaces. *Biomaterials* **28**, 3273–3283 (2007).
82. Thevenot, P., Hu, W. & Tang, L. *SURFACE CHEMISTRY INFLUENCE IMPLANT BIOCOMPATIBILITY*.
83. Bernhard, C. *et al.* Repelling and ordering: The influence of poly(ethylene glycol) on protein adsorption. *Phys. Chem. Chem. Phys.* **19**, 28182–28188 (2017).
84. Zhang, M. & Ferrari, M. Hemocompatible Polyethylene Glycol Films on Silicon. *Biomed. Microdevices* **1**, 81–89 (1998).
85. Ogura, H. *et al.* Activated platelets enhance microparticle formation and platelet-leukocyte interaction in severe trauma and sepsis. in *Journal of Trauma - Injury, Infection and Critical Care* vol. 50 801–809 (Lippincott Williams and Wilkins, 2001).
86. Cerletti, C., Tamburrelli, C., Izzi, B., Gianfagna, F. & De Gaetano, G. Platelet-leukocyte interactions in thrombosis. *Thrombosis Research* vol. 129 263–266 (2012).
87. Cerletti, C., de Gaetano, G. & Lorenzet, R. Platelet-leukocyte interactions: Multiple links between inflammation, blood coagulation and vascular risk. *Mediterranean Journal of Hematology and Infectious Diseases* vol. 2 (2010).
88. Yun, S.-H., Sim, E.-H., Goh, R.-Y., Park, J.-I. & Han, J.-Y. Platelet Activation: The Mechanisms and Potential Biomarkers. (2016) doi:10.1155/2016/9060143.
89. Damodaran, V. B. *et al.* Antithrombogenic properties of a nitric oxide-releasing dextran

- derivative: Evaluation of platelet activation and whole blood clotting kinetics. *RSC Adv.* **3**, 24406–24414 (2013).
90. Gungor, B. *et al.* Comparison of the adherence of E.Coli and S. Aureus to ten different prosthetic mesh grafts: In vitro experimental study. *Indian J. Surg.* **72**, 226–231 (2010).
91. Orapiriyakul, W., Young, P. S., Damiati, L. & Tsimbouri, P. M. Antibacterial surface modification of titanium implants in orthopaedics. *J. Tissue Eng.* **9**, 204173141878983 (2018).